Energy imbalance alters Ca²⁺ handling and excitability of POMC neurons

Lars Paeger[1,2†], Andreas Pippow[1,2†], Simon Hess[1,2], Moritz Paehler[1,2], Andreas C Klein[1,2], Andreas Husch[1,2], Christophe Pouzat[3], Jens C Brüning[2,4,5], Peter Kloppenburg[1,2]*

[1]Biocenter, Institute for Zoology, University of Cologne, Cologne, Germany; [2]Cologne Excellence Cluster on Cellular Stress Responses in Aging-Associated Diseases, University of Cologne, Cologne, Germany; [3]MAP5 - Mathématiques Appliquées à Paris 5, CNRS UMR 8145, Paris, France; [4]Department of Mouse Genetics and Metabolism, Institute for Genetics, Center of Molecular Medicine Cologne, Center for Endocrinology, Diabetes and Preventive Medicine, University Hospital of Cologne, Cologne, Germany; [5]Max Planck Institute for Metabolism Research, Cologne, Germany

*For correspondence: peter. kloppenburg@uni-koeln.de

[†]These authors contributed equally to this work

Abstract Satiety-signaling, pro-opiomelanocortin (POMC)-expressing neurons in the arcuate nucleus of the hypothalamus play a pivotal role in the regulation of energy homeostasis. Recent studies reported altered mitochondrial dynamics and decreased mitochondria- endoplasmic reticulum contacts in POMC neurons during diet-induced obesity. Since mitochondria play a crucial role in Ca²⁺ signaling, we investigated whether obesity alters Ca²⁺ handling of these neurons in mice. In diet-induced obesity, cellular Ca²⁺ handling properties including mitochondrial Ca²⁺ uptake capacity are impaired, and an increased resting level of free intracellular Ca²⁺ is accompanied by a marked decrease in neuronal excitability. Experimentally increasing or decreasing intracellular Ca²⁺ concentrations reproduced electrophysiological properties observed in diet-induced obesity. Taken together, we provide the first direct evidence for a diet-dependent deterioration of Ca²⁺ homeostasis in POMC neurons during obesity development resulting in impaired function of these critical energy homeostasis-regulating neurons.
DOI: 10.7554/eLife.25641.001

Introduction

Energy homeostasis is tightly regulated by highly dynamic neuronal networks in the hypothalamus. These control circuits adapt food intake and energy expenditure to the needs of the organism and the availability of fuel sources in the periphery of the body (*Apovian, 2016*; *Gao and Horvath, 2007*; *Power, 2012*). Dysregulation of this functional circuitry can cause metabolic disorders including obesity and type two diabetes, whose prevalence is increasing in Western societies (*Schwartz and Porte, 2005*). In the arcuate nucleus of the hypothalamus (ARH), satiety-signaling (anorexigenic), pro-opiomelanocortin (POMC)-expressing, and hunger-signaling (orexigenic) agouti-related peptide (AgRP)-expressing neurons integrate endocrine and metabolic factors to adapt neuronal activity that ultimately generates neurosecretory output (*Morton et al., 2006*; *Sohn et al., 2013*). This neurocircuitry not only regulates food intake and energy expenditure but also adapts glucose homeostasis to the acutely changing needs of the organism (*Belgardt et al., 2009*; *Blouet and Schwartz, 2010*; *Könner et al., 2007*; *Steculorum et al., 2016*).

Substantial progress has been made in identifying fuel-sensing endocrine and metabolic factors, such as leptin, insulin, glucose, free fatty acids, and uridine diphosphate (*Gao and Horvath, 2007*;
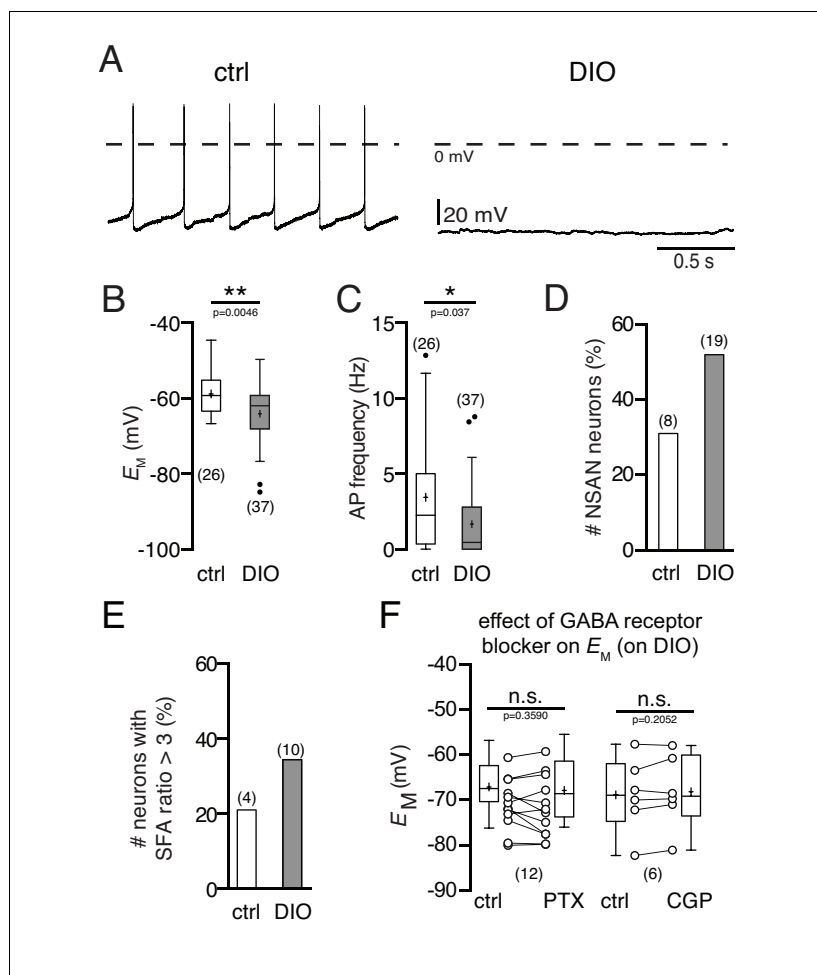
Figure 1. Diet-induced obesity decreases the spontaneous activity and hyperpolarizes the membrane potential of POMC neurons. Recordings were performed in the perforated patch-clamp configuration from eGFP expressing POMC neurons in the arcuate nucleus. (**A**) Original recordings of POMC neurons of mice on NCD and in DIO. (**B** and **C**) POMC neurons of DIO mice were hyperpolarized (**B**) and their action potential frequency was decreased (**C**) (Mann-Whitney test). (**D** and **E**) The percentage of silent (F < 0.5 Hz) POMC neurons (**D**) and the percentage of POMC neurons with strong SFA (SFA ratio >3 Hz) (**E**) was higher in DIO mice compared to controls. (**F**) The GABA$_A$ receptor blocker PTX and the GABA$_B$ receptor blocker CGP54626 did not restore the membrane potential of DIO mice to control (paired t-test). SFA, spike frequency adaptation. **p<0.01, ***p<0.001.
DOI: 10.7554/eLife.25641.002

Jordan et al., 2010; *Steculorum et al., 2015*; *Varela and Horvath, 2012*), and many immediate actions of these hormones and nutrient components on POMC and AgRP neurons are well understood (*Claret et al., 2007*; *Jo et al., 2009*; *Parton et al., 2007*; *Spanswick et al., 1997*, *2000*).

In contrast, we have only limited information about the effects of sustained extreme nutritional states, such as high caloric intake and obesity, on the cellular electrophysiological properties and performance of these cells. It is well documented that increased caloric intake causes leptin and insulin resistance in ARH neurons (*Könner and Brüning, 2012*; *Varela and Horvath, 2012*), and that glucose sensing of POMC neurons is impaired in obesity (*Parton et al., 2007*). In POMC neurons, which are activated by reactive oxygen species (ROS), high-fat feeding promoted proliferation of peroxisomes and in turn reduced ROS levels and action potential firing (*Diano et al., 2011*). Increased expression of the suppressor of cytokine signaling (SOCS-3) has been shown to desensitize neurons to the anorexigenic actions of leptin and insulin (*Bjørbaek et al., 1998*; *Ueki et al., 2004*), and we and others have demonstrated that inflammatory signals activated by a high-fat diet cause neuronal leptin and insulin resistance (*Belgardt et al., 2010*; *Dietrich et al., 2013*;

Kleinridders et al., 2009; *Schneeberger et al., 2013*; *Tsaousidou et al., 2014*). Correspondingly, endoplasmic reticulum (ER) stress was recognized as an important causal factor for the development of leptin resistance (*Hosoi et al., 2008*; *Ramírez and Claret, 2015*). Most recent studies have identified mitofusin-2 (MFN2) as a direct link between ER stress and leptin resistance in the hypothalamus (*Schneeberger et al., 2013*). In anorexigenic POMC neurons diet-induced obesity (DIO) altered mitochondrial network dynamics and decreased mitochondria-ER contacts by downregulation of MFN2. It is important to note that this is a cell type-specific response, when compared to the functionally antagonistic orexigenic AgRP neurons in the ARH (*Dietrich et al., 2013*; *Schneeberger et al., 2013*). Since mitochondrial function is intimately linked to the dynamic behavior of these organelles, and since mitochondria play a crucial role in intracellular Ca^{2+} signaling (*Szabadkai and Duchen, 2008*), we asked if intracellular Ca^{2+}-handling properties are modulated in POMC neurons under DIO.

This question is especially interesting, since several lines of evidence suggest that age-dependent changes in Ca^{2+} homeostasis may partially increase, or even cause, the susceptibility for age-dependent impairment of neuronal function and neurodegeneration (*Berridge, 2012*; *Marambaud et al., 2009*; *Toescu and Verkhratsky, 2007*). Here, increased Ca^{2+} load on the cell can result in neurotoxicity and impaired neuronal function (*Rizzuto et al., 2012*; *Rowland and Voeltz, 2012*; *Surmeier et al., 2010*). Thus, to assess whether Ca^{2+} handling and the function of satiety-mediating POMC neurons are altered in diet-induced obesity, we analyzed the Ca^{2+}-handling properties of these neurons and their intrinsic electrophysiological characteristics in detail. We found that diet-induced obesity impaired intracellular Ca^{2+} handling, including mitochondrial Ca^{2+} uptake. The changes in Ca^{2+} handling were accompanied by a marked decrease in activity and excitability of POMC neurons. Experimentally increasing or decreasing intracellular Ca^{2+} concentrations reproduced the electrophysiological properties observed in diet-induced obesity.

Results

### High-fat diet decreases activity of anorexigenic POMC neurons

To investigate the effects of diet-induced obesity (DIO) on the intrinsic electrophysiological characteristics of POMC neurons, we performed electrophysiological recordings on identified POMC neurons of 18-week-old transgenic mice expressing GFP under the control of the *Pomc* promoter (*Cowley et al., 2001*). The animals had been fed a normal chow diet (NCD) or a high-fat diet (HFD) for 12 weeks, starting at an age of six weeks. In an independent experiment we measured increase in body weight and body fat content during HFD exposure. Mice exposed to 11–13 weeks of HFD-feeding (starting at an age of 6 weeks) showed an elevation in body weight (control: 29.3 ± 1.9 g, n = 25; DIO: 38.6 ± 4.1 g, n = 25; p<0.0001, Mann-Whitney test) and body fat content (control: 12.7 ± 4.2%, n = 25; DIO: 32.1 ± 4.0%, n = 25; p<0.0001, Mann-Whitney test) compared to NCD-fed controls.

Using perforated patch recordings, the integrity of intracellular components was ensured. The activity of POMC neurons of mice exposed to a HFD was clearly reduced, which is in line with previous results (*Jo et al., 2009*). The membrane potential was hyperpolarized (*Figure 1A,B*; control: −58.8 ± 1.1 mV, n = 26; DIO: −64.0 ± 1.2 mV, n = 37; p=0.0046, Mann-Whitney test) and the spontaneous activity was decreased (*Figure 1A,C*; control: 3.4 ± 0.7 Hz, n = 26; DIO: 1.7 ± 0.4 Hz, n = 37; p=0.037, Mann-Whitney test). Moreover, the percentage of POMC neurons without spontaneous action potential firing (NSAN, not spontaneously active neuron; F < 0.5 Hz) increased from 31% (8 of 26) in control mice to 51% (19 of 37) in DIO mice (*Figure 1D*). Likewise, the number of POMC neurons with strong spike frequency adaptation was markedly enhanced, i.e., the percentage of neurons with a spike frequency adaptation ratio (SFA, for details see Materials and methods) >3 increased from 21% (4 of 19) in the control group to 34% (10 of 29) in the DIO group (*Figure 1E*).

Previous studies reported changes in both glutamatergic and GABAergic synaptic innervation of POMC neurons during a sustained HFD (*Klöckener et al., 2011*; *Newton et al., 2013*). Since all our experiments were performed in the presence of ionotropic synaptic blockers (for details see Materials and methods), it is unlikely that the observed hyperpolarization of the membrane potential in POMC neurons was caused by changes in synaptic input. However, to define the effect of potentially altered GABAergic input on POMC neurons in DIO, we performed two sets of experiments. Whole-

cell voltage-clamp recordings revealed that the inhibitory postsynaptic current frequency was increased in DIO. Application of picrotoxin (100 µM), a GABA$_A$ receptor antagonist, and CGP54626 (50 µM), a GABA$_B$ receptor antagonist, blocked GABAergic currents and eliminated IPSCs completely (data not shown). However, neither picrotoxin nor CGP54626 restored the membrane potential and firing rate to control levels (*Figure 1F*; PTX: n = 12, p=0.3590; CGP: n = 6; p=0.2052; paired t-tests). The results show that the DIO-induced hyperpolarization and the decrease in firing rate cannot be exclusively attributed to the increase in inhibitory input organization of these cells, but are also a consequence of altered cell-intrinsic properties.

Overall, we found that POMC neurons without spontaneous activity had a two-fold higher SFA ratio than spontaneously firing POMC neurons (*Figure 2A–C*; POMC firing: 2.0 ± 0.1, n = 27; POMC silent: 3.6 ± 0.3, n = 22, p<0.0001, Mann-Whitney test). This was particularly reflected in a strong reduction of the action potential number over the time course of the depolarizing stimulus
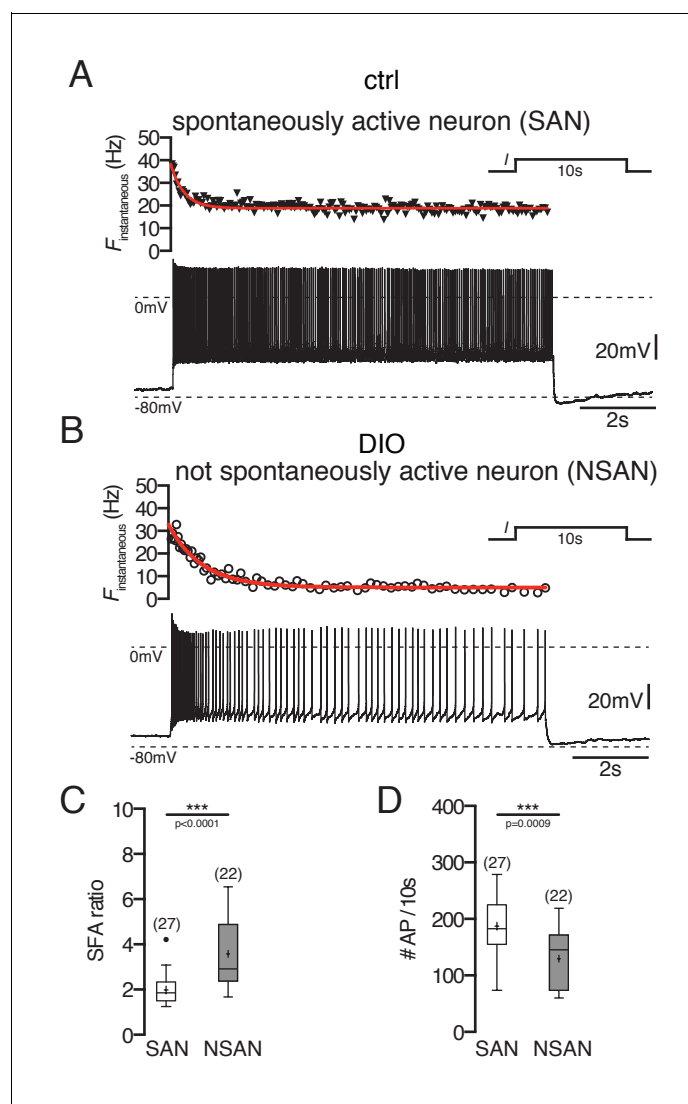
Figure 2. Spike frequency adaptation of POMC neurons is stronger in DIO mice. (**A and B**) Original recording (bottom) and the corresponding instantaneous spike frequency plot (top) of a spontaneously firing (**A**) and silent (**B**) POMC neuron during a 10 s depolarizing current injection. (**C and D**) SFA ratios are higher in silent POMC neurons (**C**) and, accordingly, the number of APs during the 10 s depolarization decreased (**D**) (Mann-Whitney test). SFA, spike frequency adaptation; SAN, spontaneously active neuron; NSAN, not spontaneously active neuron (F < 0.5 Hz). ***p<0.001.
DOI: 10.7554/eLife.25641.003

(*Figure 2D*; POMC firing: 188 ± 10, n = 25; POMC silent: 130 ± 11.0, n = 22; p=0.0009, Mann-Whitney test).

Collectively, these data show that in DIO mice, the excitability of anorexigenic POMC neurons is markedly reduced.
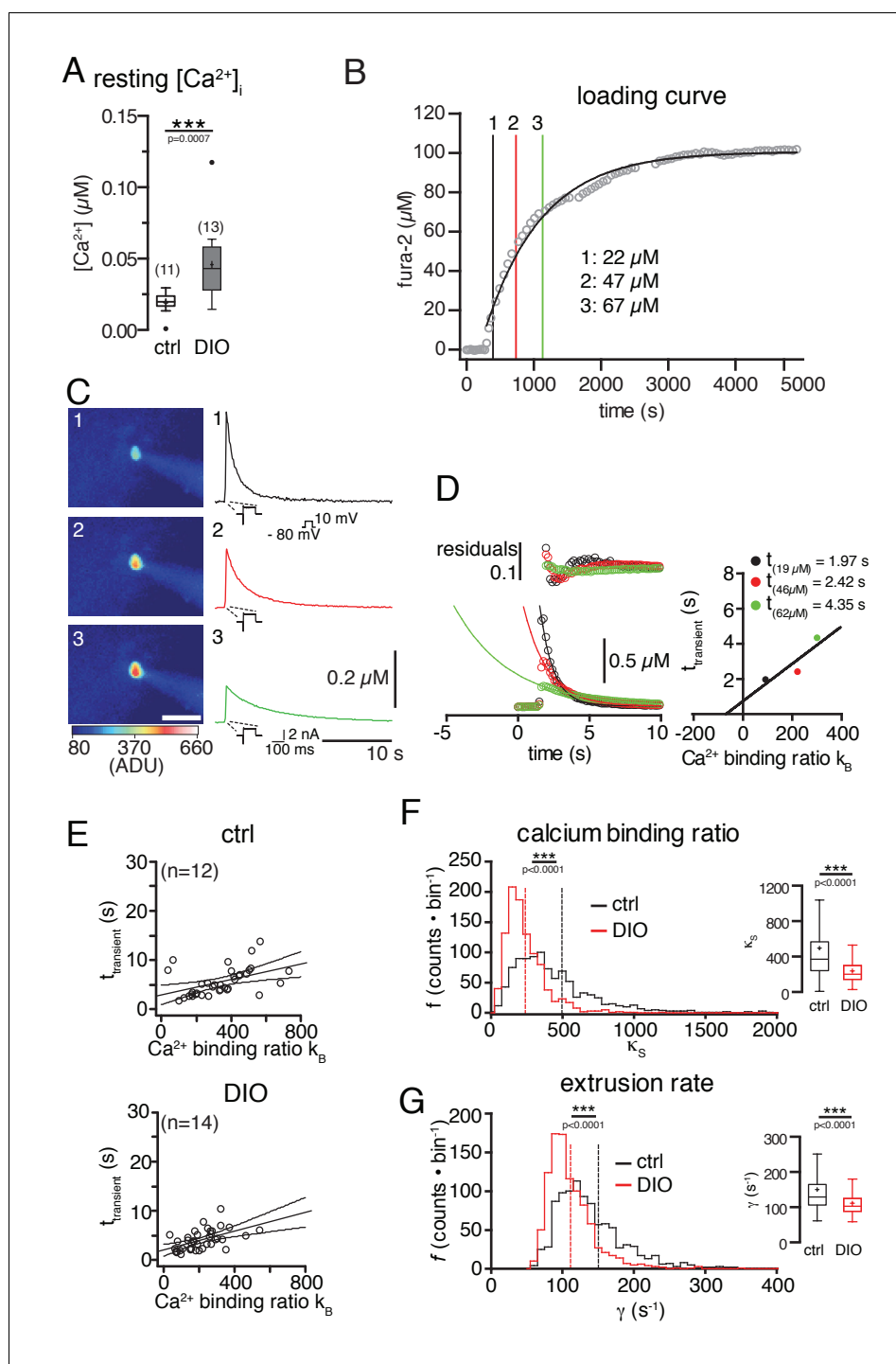
DIO alters Ca²⁺ handling of POMC neurons

Further, we compared the Ca^{2+}-handling properties of POMC neurons, which represent a critical determinant of neuronal activity, of control and DIO mice, by using ratiometric Ca^{2+} imaging with fura-2 (*Grynkiewicz et al., 1985*). Surprisingly, these experiments revealed increased levels of free intracellular Ca^{2+} in POMC neurons in DIO compared to control mice (*Figure 3A*; control: 19.3 ± 2.3 nM, n = 11; DIO: 45.8 ± 7.3 nM, n = 13; p=0.0007, Mann-Whitney test), which was not expected, because of the DIO-induced hyperpolarization and decreased activity of the neurons.

Based on this finding, we next analyzed changes in Ca^{2+}-handling properties of POMC neurons. Since the dynamics of free intracellular Ca^{2+} concentrations strongly depend on the endogenous Ca^{2+}-buffering capacity and the Ca^{2+} extrusion rate, we also investigated whether DIO induces changes in the Ca^{2+}-handling parameters of POMC neurons by using the 'added buffer approach' in combination with whole-cell patch-clamp recordings and optical Ca^{2+} imaging (*Neher and Augustine, 1992*; *Pippow et al., 2009*). The added buffer approach is based on a single compartment model with the rationale that for measurements of intracellular Ca^{2+} concentrations with Ca^{2+} chelator-based indicators, the amplitude and time course of the signals depend on the concentration of the Ca^{2+} indicator (here: fura-2). The indicator acts as an exogenous Ca^{2+} buffer and competes with the endogenous Ca^{2+} buffer(s).

The kinetics of cytosolic Ca^{2+} signals strongly rely on the endogenous and exogenous (added) Ca^{2+} buffers of the cell. The amplitude and decay rate of free intracellular Ca^{2+} changes with the increasing exogenous buffer concentration; the amplitude of free Ca^{2+} decreases, and the time constant $\tau_{transient}$ of the decay increases, as shown in *Figure 3C and D*. If the buffer capacity of the added buffer is known, the time constant of the decay ($\tau_{transient}$; *Figure 3D*) can be used to estimate, by extrapolation, the Ca^{2+} signal to conditions, with only endogenous buffers are present (-κ_B = 1 + κ_S). The model used for this study (see *Equation 4*) assumes that the decay time constants $\tau_{transient}$ are a linear function of the Ca^{2+}-binding ratios (κ_B and κ_S) (*Neher and Augustine, 1992*). The ratio κ_S was determined from the negative x-axis intercept of the plot shown in *Figure 3E*. The slope of the fit is the inverse of the linear extrusion rate (γ). The point of intersection of the linear fit with the y-axis denotes the endogenous decay time constant τ_{endo} (no exogenous Ca^{2+} buffer in the cell). To estimate the variability of these parameters, which were determined by linear fits, we used a bootstrap approach (n = 1000; as described in the Materials and methods). Using this method, we found that the endogenous Ca^{2+}-binding ratio (*Figure 3F*; control: 497 ± 18; DIO: 240 ± 5; p=0.0001, unpaired t-test), and, simultaneously, the Ca^{2+} extrusion rate (*Figure 3G*; control: 150 ± 3 s^{-1}; DIO: 111 ± 1 s^{-1}; p<0.0001; unpaired t-test) were reduced in POMC neurons of DIO mice compared to control mice.

DIO reduces mitochondrial Ca²⁺ content of POMC neurons

Since mitochondria play a crucial role in intracellular Ca^{2+} handling, we investigated whether the mitochondrial capacity of POMC neurons to accumulate Ca^{2+} was affected in DIO mice (*Santo-Domingo and Demaurex, 2010*; *Szabadkai and Duchen, 2008*). This was achieved by determining the Ca^{2+} release induced by the protonophore FCCP, as a measure for the ability of the mitochondria to contribute to the regulation of intracellular Ca^{2+}. Brain slices were AM-loaded with fura-2, and mitochondrial Ca^{2+} release was induced in GFP-expressing POMC neurons by bath application of FCCP for 2 min (2 μM; *Figure 4A*). To monitor the Ca^{2+} release, we recorded the fluorescence ratio (F340/F380) (*Figure 4B*), which is proportional to an increase in free cytosolic calcium ([Ca²⁺]ᵢ). FCCP induced a lower elevation of free cytosolic Ca^{2+} in the DIO (Δ F340/F380 = 0.012 ± 0.001, n = 72 cells, N = 11 brain slices) than in the control cohort (Δ F340/F380 = 0.020 ± 0.003, n = 46 cells, N = 10 brain slices) (*Figure 4B,C*; p=0.0406, unpaired t-test). This indicates a reduced mitochondrial capacity to accumulate Ca^{2+} in POMC neurons of DIO mice.

Figure 3. Diet-induced obesity changes the endogenous Ca^{2+}-handling properties of POMC neurons. Ca^{2+} handling was analyzed using a combination of patch-clamp recordings, ratiometric Ca^{2+} imaging, and the 'added buffer approach'. (**A**) Ca^{2+} resting level. The concentration of free cytosolic Ca^{2+} was increased in DIO mice. (**B–G**) Ca^{2+}-handling properties. (**B**) fura-2 loading curve. POMC neurons were loaded via the patch pipette with the ratiometric Ca^{2+} indicator fura-2, which also serves as the added Ca^{2+} buffer. Fura-2 fluorescence was acquired at 360 nm excitation (isosbestic point of fura-2) every 30 s, and converted into fura-2 concentrations. (**C**) Decay kinetics of voltage-induced Ca^{2+} transients of the POMC neuron in (**B**). The images (left panels) were acquired at times indicated in (**B**) and demonstrate the increasing fura-2 concentration during loading. The graphs (right panels) demonstrate the effect of increasing added Ca^{2+} buffer (fura-2) concentrations on the decay kinetics of voltage-evoked Ca^{2+} transients. (**C and D**) Analysis of endogenous Ca^{2+}-handling parameters in a single cell. With

Figure 3 continued on next page

increasing fura-2 concentrations, the amplitudes of transients decreased, and the time constants ($\tau_{transient}$) for decay were prolonged (**C and D**). The decay time constants were plotted against the Ca^{2+}-binding ratios of fura-2 (κ_B) (**D**). κ_B was calculated from the intracellular fura-2 concentration, the K_d of fura-2, and the resting concentration of free intracellular Ca^{2+}. The solid line represents the linear fit to the data. An estimate of κ_S was obtained as the negative x-axis intercept. The Ca^{2+} extrusion rate is estimated from the slope of the fit and the endogenous decay time constant from the intercept with the y-axis. (**E**) The decay time constants of all recorded neurons were plotted as a function of κ_B for all POMC neurons of the control and DIO mice. The best linear fits with 95% confidence bands are shown. (**F and G**) To estimate the variance of the endogenous Ca^{2+}-binding ratio (κ_S) and the extrusion rate (γ), we used a bootstrap method (1000 samples), which provided bootstrap distributions (n = 1000) of the parameters for the control and DIO mice. Vertical lines indicate the means. (**F**) Distributions of κ_S. Sixteen counts for the control and one count for the DIO cohort between 2000 and 7500 are not shown. (**G**) Distribution of γ. Eighteen counts for the control and one count for the DIO cohort between 400 and 1350 are not shown. Subsequently, the distributions were log-transformed to bring them closer to a Gaussian, before applying unpaired t-tests. ***p<0.001.

Spike frequency adaptation is increased in silent POMC neurons

Since the DIO-induced decrease in POMC neuron activity and excitability coincided with elevated levels of free intracellular Ca^{2+}, we hypothesized that both findings are linked and that the elevated Ca^{2+} levels might cause the DIO-induced inhibition of POMC neurons. To verify this hypothesis, we
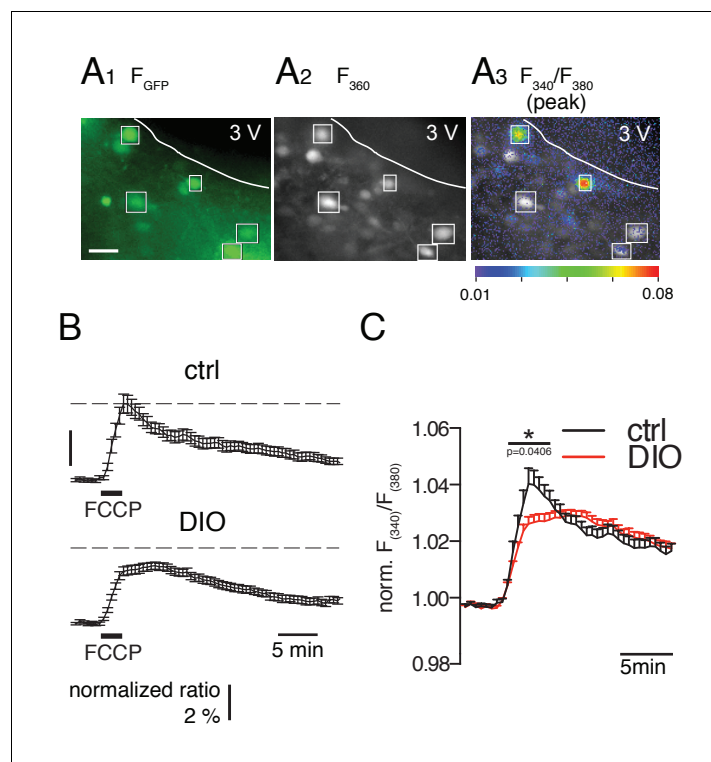
Figure 4. FCCP-induced mitochondrial Ca^{2+} release is smaller in POMC neurons of DIO mice. (**A**) GFP-labeled POMC neurons (**A1**) and fura-2 fluorescence of AM-loaded neurons in a brain slice before (**A2**) and during (**A3**) FCCP (2 µM, 2 min) bath application. Regions of interests indicate double-labeled neurons, which were used for analysis. Scale bar: 50 µm. (**B**) Time course of FCCP-induced increase in intracellular Ca^{2+} concentration [as $\Delta(F_{340}/F_{380})/(F_{340}/F_{380})_0$] in POMC neurons of control and DIO mice. (**C**) For better visualization and comparison between the two populations, the fluorescence ratio of each recorded neuron was normalized to its baseline. The overlay in the right panel shows the release and uptake in higher resolution. Control, n = 46 cells, N = 10 brain slices. DIO, n = 72 cells, N = 11 brain slices. *p<0.05; Mann-Whitney test.
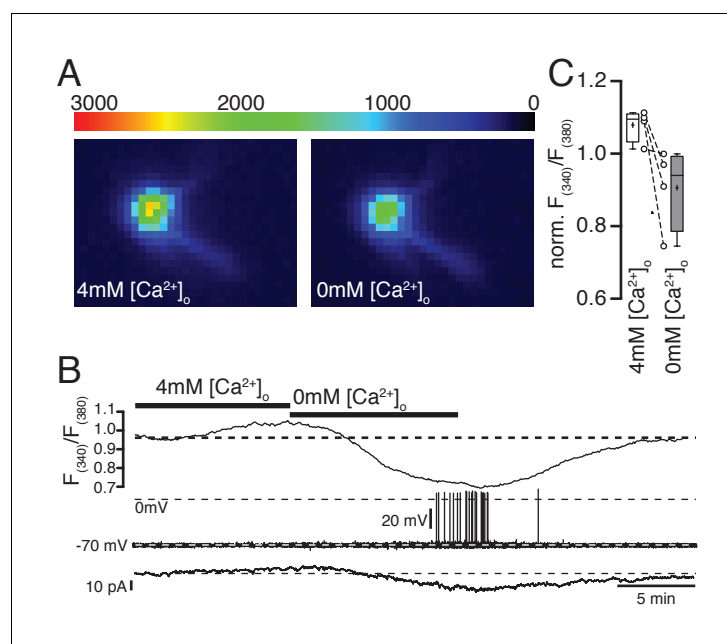
modified the intracellular Ca^{2+} concentration by changing the extracellular Ca^{2+} concentration and tested if the changes in intrinsic electrophysiological properties observed in DIO can be reproduced by changing the intracellular Ca^{2+} concentration.

To confirm that changes in extracellular Ca^{2+} concentration indeed affect free intracellular Ca^{2+} levels, we combined electrophysiological recordings and ratiometric Ca^{2+} imaging with fura-2. An example experiment is shown in *Figure 5A–C*. To prevent indirect (activity-induced) changes in intracellular Ca^{2+} concentrations, the neurons were clamped at −70 mV with low-frequency voltage-clamp (implemented in an EPC10 patch-clamp amplifier, HEKA, Lambrecht, Germany). Elevating extracellular Ca^{2+} concentrations from 2 mM to 4 mM increased intracellular Ca^{2+} levels and decreased the hyperpolarizing holding current (*Figure 5B*). In contrast, reducing extracellular Ca^{2+} caused a drop in free intracellular Ca^{2+}, increased the hyperpolarizing holding current, and even induced the generation of action potentials (*Figure 5A–C*). Using this direct approach to decrease or increase intracellular Ca^{2+} levels, we investigated if the DIO-induced changes in excitability can be directly mimicked by adjusting the levels of free intracellular Ca^{2+}.

As hypothesized, reducing intracellular Ca^{2+} depolarized the membrane potential and led to the generation of spontaneous action potentials in silent POMC neurons (*Figure 6A,C*). Increasing intracellular Ca^{2+} reduced the action potential frequency in neurons that were spontaneously active (*Figure 6B,D*). It is important to note that this is not a general effect, that is, removing extracellular Ca^{2+} did not change the intrinsic electrophysiological properties of hippocampal CA1 pyramidal cells of rats (*Penn et al., 2016*; *Su et al., 2001*). Reducing intracellular Ca^{2+} concentrations in silent POMC neurons decreased the elevated SFA ratios to control levels of spontaneously active POMC neurons (*Figure 7A–C*). In neurons with spontaneous activity the SFA ratio decreased upon reducing the intracellular Ca^{2+} concentration (*Figure 7C*). As a consequence of the reduced SFA, the number of action potentials per 10 s depolarizing current pulse was larger with low $[Ca^{2+}]_i$ (*Figure 7D*).

Moreover, we determined the current at which action potentials were generated (threshold current, $I_{threshold}$) by using ascending current ramps. In silent POMC neurons $I_{threshold}$ was higher compared to spontaneously active neurons, reflecting the decreased excitability of these cells

Figure 5. Ratiometric Ca^{2+} imaging with fura-2 shows that increasing or decreasing extracellular Ca^{2+} concentrations increases or decreases intracellular Ca^{2+} levels, respectively. (A,B,C) Removal of extracellular Ca^{2+} decreased intracellular Ca^{2+} levels concomitant with an increase in hyperpolarizing holding current (B) when cells were clamped to −70 mV (low-frequency voltage-clamp). Note the generation of spontaneous action potentials in low Ca^{2+} conditions. (C) Changes of intracellular Ca^{2+} levels (normalized fura-2 ratios) under normal, high, and low Ca^{2+} conditions (n = 4).
DOI: 10.7554/eLife.25641.006
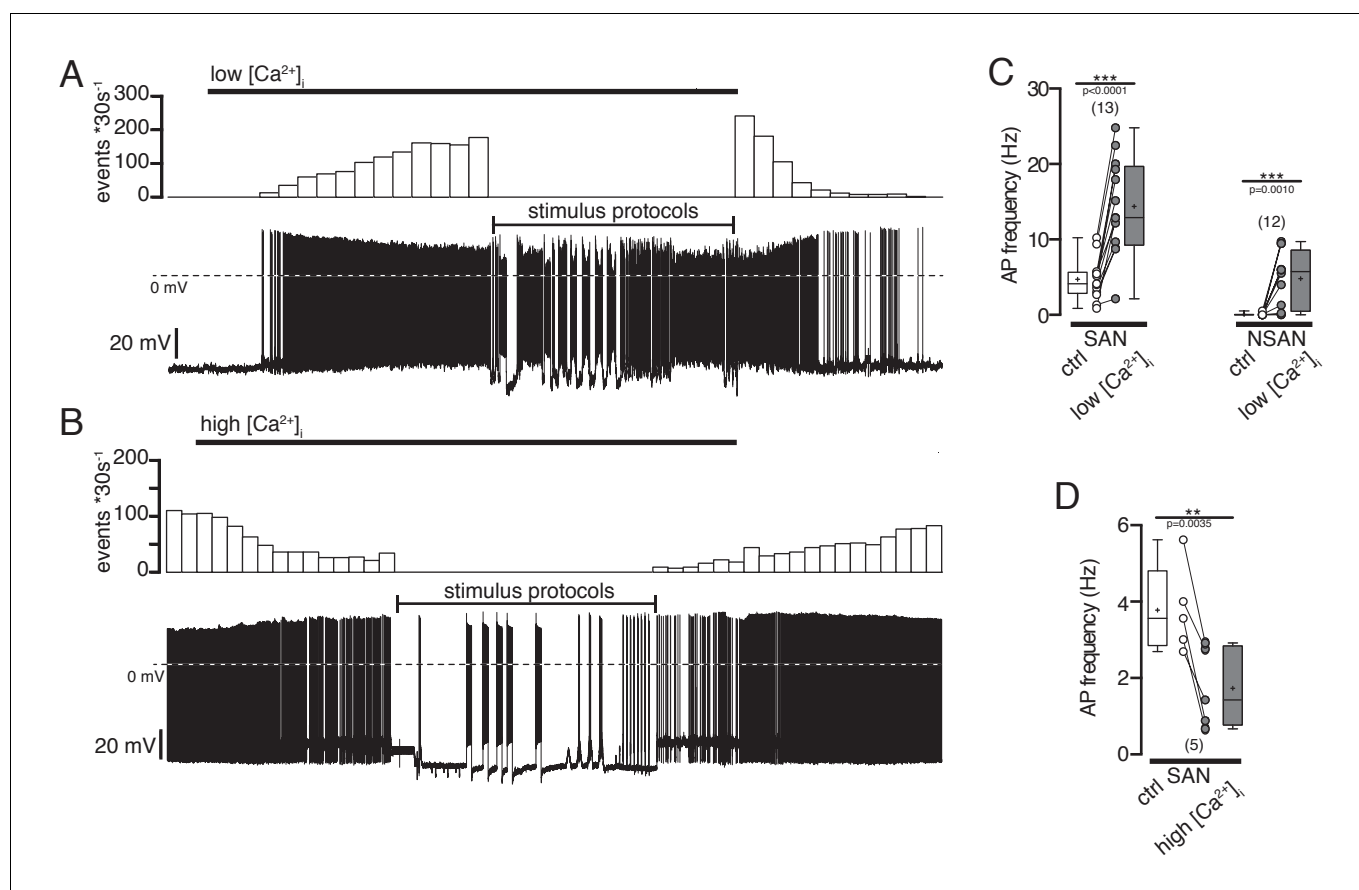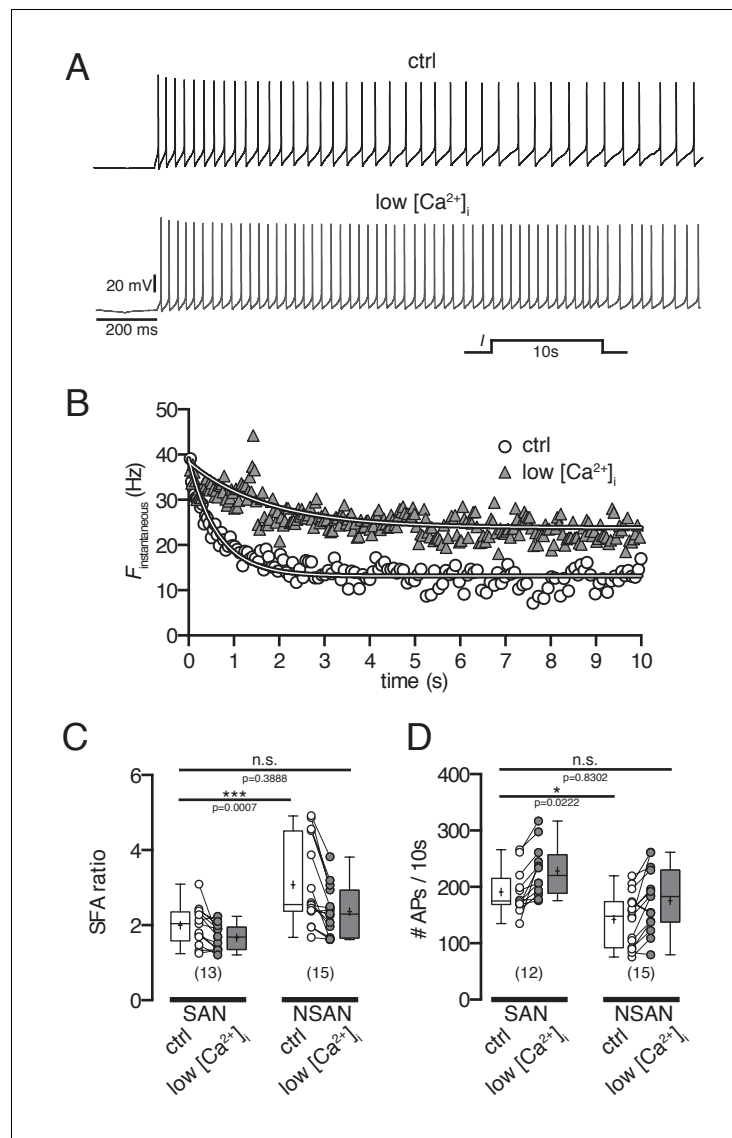
Figure 6. Effect of intracellular Ca^{2+} concentrations on action potential frequency of POMC neurons. (**A and B**) Original recordings of POMC neurons illustrating the effect of decreasing or increasing intracellular Ca^{2+} concentrations. (**A**) A silent POMC neurons started to generate action potentials with decreasing $[Ca^{2+}]_i$. The effect reverted to control levels at normal $[Ca^{2+}]_i$. (**B**) In a spontaneously active neuron, the AP frequency was reduced with increasing $[Ca^{2+}]_i$. The effect reversed at normal Ca^{2+} levels. (**C**) Action potential frequency of spontaneously active and silent POMC neurons at normal and low $[Ca^{2+}]_i$, respectively (paired t-test). (**D**) Action potential frequency of spontaneously active neurons at normal and high $[Ca^{2+}]_i$, respectively (paired t-test). SAN, spontaneously active neuron; NSAN, not spontaneously active neuron (F < 0.5 Hz). **p<0.01, ***p<0.001.
DOI: 10.7554/eLife.25641.007

(*Figure 8A,B*). Decreasing $[Ca^{2+}]_i$ reduced $I_{threshold}$ in both firing and silent POMC neurons to similar values (*Figure 8A,B*). In line with these experiments, *current-frequency* relations were steeper in firing neurons compared to silent POMC neurons, and decreasing $[Ca^{2+}]_i$ increased the *current-frequency* relation to the same level in all cells (*Figure 8C*).

SK channels contribute to decreased excitability of POMC neurons in DIO

Based on the findings that DIO increased the Ca^{2+} resting level and hyperpolarized the membrane potential, we hypothesized that activation of Ca^{2+}-dependent K^+ currents ($I_{K(Ca)}$) might contribute to the observed hyperpolarization and decreased neuronal activity. To verify this hypothesis, we used blockers for specific components of $I_{K(Ca)}$ and assessed if the changes in intrinsic electrophysiological properties, which we observed in silenced neurons and which were accompanied by elevated $[Ca^{2+}]_i$, can be reversed. We applied the toxins apamin, charybdotoxin, iberiotoxin, and paxilline, which have been shown to block specific components of $I_{K(Ca)}$ in vertebrates (*Bennett et al., 2000*; *Blatz and Magleby, 1986*; *Faber and Sah, 2003*; *Fioretti et al., 2004*; *Galvez et al., 1990*; *Ghatta et al., 2006*; *Giangiacomo et al., 1992*; *Kaczorowski et al., 1996*; *Pineda et al., 1992*; *Wolfart et al., 2001*; *Sanchez and McManus, 1996*; *Li and Cheung, 1999*; *Zhou and Lingle, 2014*). Apamin blocks SK ($K_{Ca} 2.1$, $K_{Ca} 2.2$, $K_{Ca} 2.3$) channels, and iberiotoxin and paxilline blocks BK

Figure 7. Spike frequency adaptation in POMC neurons depends on intracellular Ca^{2+} concentrations. (**A and B**) Original recording (**A**) and corresponding plot of the instantaneous spike frequency (**B**) of a silent POMC neuron showing the SFA during a 10 s depolarizing current pulse at normal and reduced $[Ca^{2+}]_i$. Reducing $[Ca^{2+}]_i$ decreased the SFA. (**C**) SFA ratios of spontaneously firing and silent POMC neurons at different $[Ca^{2+}]_i$. In silent POMC neurons, the SFA is higher compared to firing POMC neurons. Reducing $[Ca^{2+}]_i$ in silent neurons decreases SFA ratios to levels of firing neurons (ANOVA with Bonferroni corrections). (**D**) The number of action potentials during the 10 s depolarizing current pulse is smaller in silent compared to firing POMC neurons. Reducing $[Ca^{2+}]_i$ increased the number of APs in silent neurons to the level of firing neurons (ANOVA with Bonferroni corrections). SFA, spike frequency adaptation; SAN, spontaneously active neuron; NSAN, not spontaneously active neuron (F < 0.5 Hz). *p<0.05, ***p<0.01.

DOI: 10.7554/eLife.25641.008

(K_{Ca} 1.1) channels. Charybdotoxin not only blocks BK (K_{Ca} 1.1) channels but has also been shown to block IK (K_{Ca} 3.1) and K_V (K_V 1.2; K_V 1.3) channels.

Bath-application of the BK channel blockers charybdotoxin (100 nM, n = 17), iberiotoxin (100 nM, n = 7) and paxilline (10 µM, n = 6) did not have reproducible effects on membrane potential, SFA or threshold currents to generate action potentials in silent, hyperpolarized POMC neurons (data not shown). In contrast, the SK channel blocker apamin (100–200 nM) had clear excitatory effects on these neurons, inducing depolarization and action potential firing in most of the silent POMC
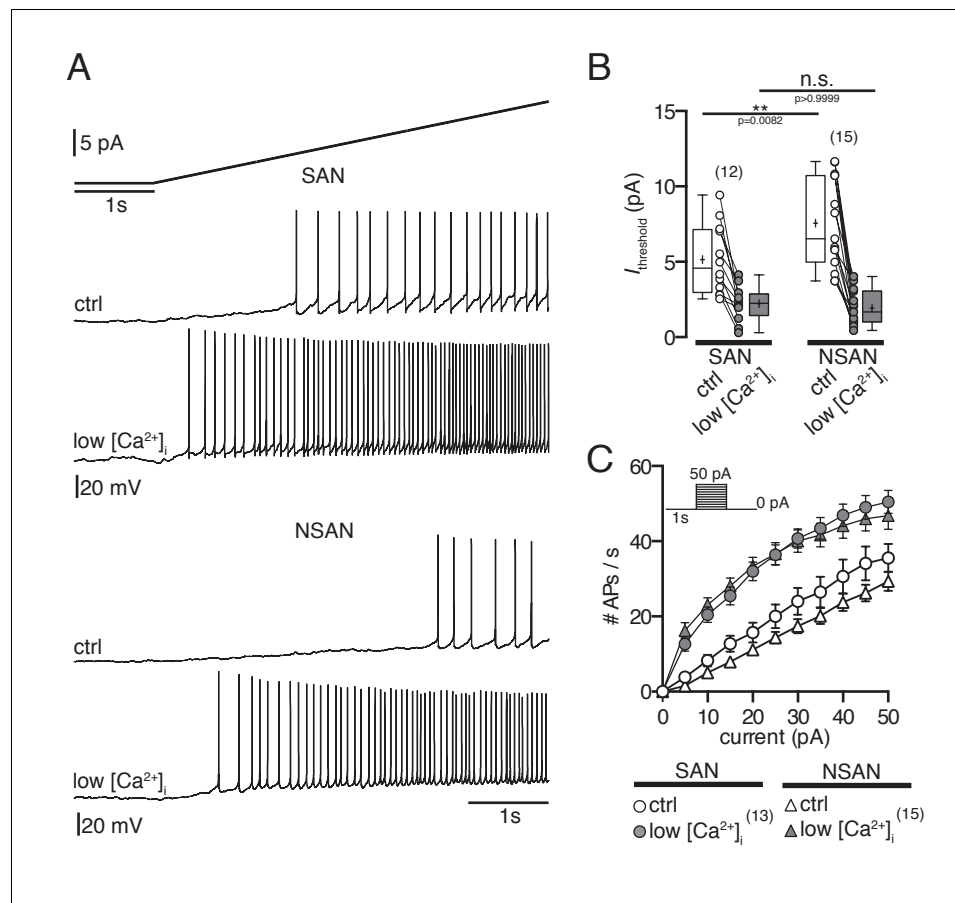
Figure 8. Low intracellular Ca^{2+} concentrations increase excitability in POMC neurons. (**A and B**) Spontaneously active neurons have a lower threshold current than silent neurons to elicit action potentials. Reducing $[Ca^{2+}]_i$ decreased $I_{threshold}$ of silent and spontaneously active neurons to similar levels (ANOVA with Bonferroni analysis). (**C**) Number of action potentials during the current pulse as a function of injected current. Under control $[Ca^{2+}]_i$, the excitability is higher in spontaneously active neurons compared to silent POMC neurons (open symbols). Reducing $[Ca^{2+}]_i$ increased the excitability of all neurons to similar levels. SAN, spontaneously active neuron; NSAN, not spontaneously active neuron (F < 0.5 Hz). *p<0.05.
DOI: 10.7554/eLife.25641.009

neurons (*Figure 9A–C*). Likewise, it reduced the SFA (*Figure 9D–F*) and decreased the threshold current for generation of action potentials in silent neurons, but not in spontaneously active control neurons.

Taken together, these blocker experiments suggest that SK channels are an import link between increased intracellular Ca^{2+} levels and decreased excitability of POMC neuron in DIO. It is not surprising that the BK channel blockers did not depolarize silent neurons, since BK channels are highly voltage dependence (*Sah and Davies, 2000*) and might not contribute to the resting membrane potential. Interestingly, the SK channel blocker apamin, but not the BK channel blockers decreased SFA in silent neurons, suggesting that SK channels contribute markedly to SFA in silent POMC neurons, as shown for various cell types (*Brenner et al., 2005*; *Vandael et al., 2012*; *Yen et al., 1999*).

In summary, we show that DIO impairs the cellular Ca^{2+}-handling properties of POMC neurons and increases the resting level of free intracellular Ca^{2+}. In agreement with these general functional changes, we found the mitochondrial Ca^{2+} content to be diminished. The changes in intracellular Ca^{2+} handling properties were accompanied by membrane hyperpolarization and a marked decrease in excitability. By experimentally changing intracellular Ca^{2+} concentrations we could reproduce the electrophysiological properties observed in DIO. Taken together, we provide the first
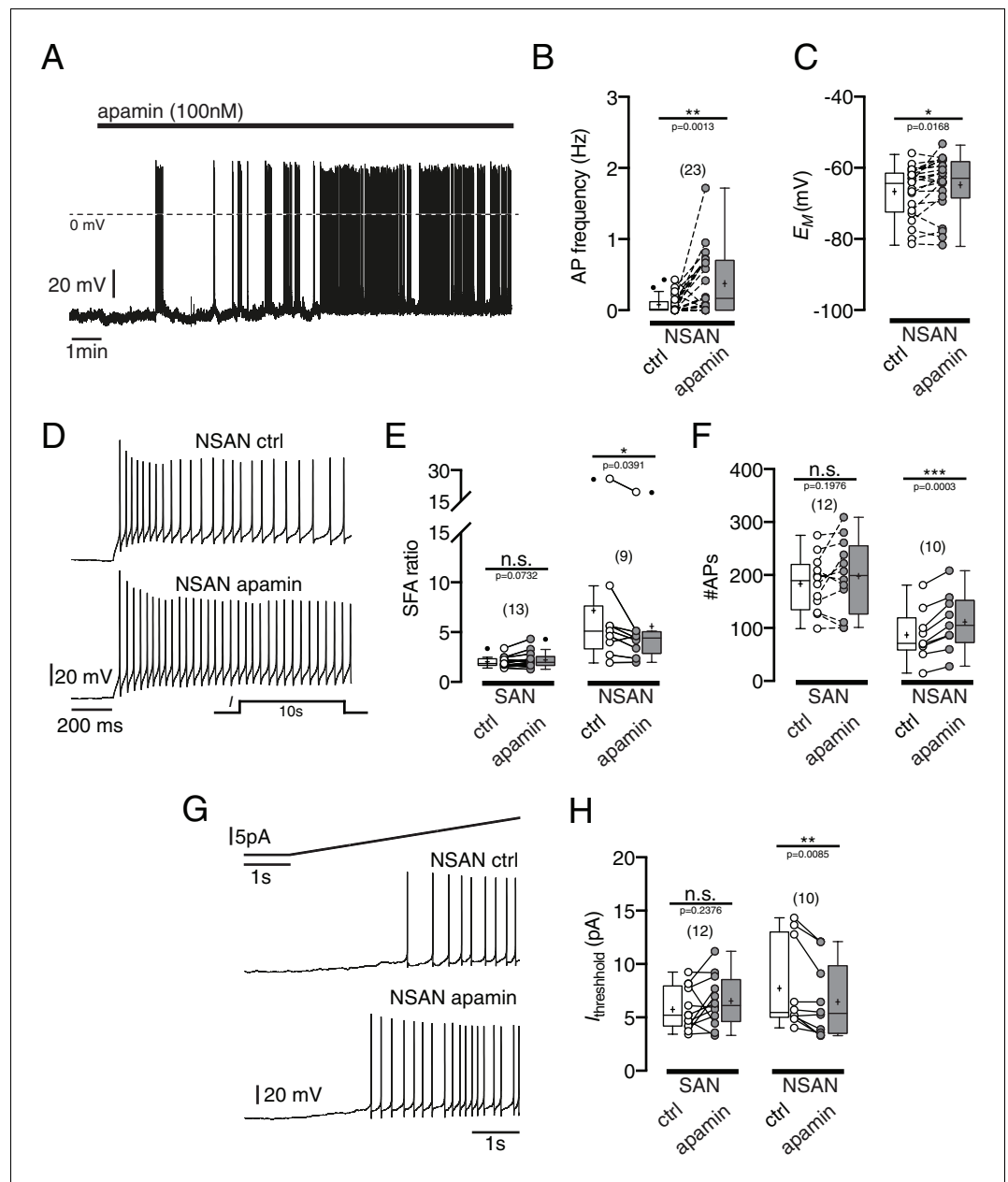
Figure 9. Blocking SK currents by apamin changes intrinsic electrophysiological properties of silent POMC neurons. (**A, B, C**) The SK channel blocker apamin (100 nM) induced depolarization and action potential firing. (**A**) A silent POMC neuron depolarized and started to generate action potentials under apamin. Action potential frequency (**B**) and membrane potential (**C**) before and during apamin application. (**D, E, F**) Apamin decreased spike frequency adaptation in silent neurons. (**D**) Original recording of a silent POMC neuron. Apamin reduced the SFA ratio (**E**) and increased the number of action potentials (**F**) during depolarization in silent but not in spontaneously active neurons. (**G, H**) Apamin reduced $I_{threshold}$ only in silent POMC neurons. (**G**) Recording of a silent POMC neuron. (**H**) Quantification of the apamin effect on $I_{threshold}$. SAN, spontaneously active neuron; NSAN, not spontaneously active neuron (F < 0.5 Hz). Paired t-test. *p<0.05, **p<0.01, ***p<0.001.
DOI: 10.7554/eLife.25641.010

direct evidence for a diet-dependent deterioration of Ca^{2+} homeostasis in POMC neurons during obesity development.

Discussion

Satiety-signaling anorexigenic POMC neurons in the ARH play a pivotal role in the regulation of energy homeostasis. While the acute physiological role of various hormones and nutrients and their signaling mechanisms in the CNS are increasingly well understood (*Gao and Horvath, 2007*; *Morton et al., 2006*; *Power, 2012*; *Schwartz and Porte, 2005*), the effects of sustained high caloric intake and obesity on these circuits remain elusive. However, defining diet-associated changes in this network and elucidating their cellular and molecular mechanisms is critical to further unravel the mechanisms leading to increased susceptibility to metabolic disorders. The present study has clearly established that the intrinsic physiological state of anorexigenic POMC neurons is markedly altered in DIO. The starting point for this study was recent work that reported POMC neuron-specific alterations in mitochondrial morphology and decreased mitochondria-ER contacts in DIO by downregulation of MNF2 expression (*Schneeberger et al., 2013*). Mitochondrial shape changes influence the activity of mitochondria and can thus have dramatic effects on cellular signaling. Since mitochondria play a crucial role in intracellular Ca^{2+} handling, we tested if Ca^{2+} handling of POMC neurons is altered in DIO. DIO caused a reduction in Ca^{2+}-buffer capacity, a reduction in Ca^{2+} extrusion rate, and an elevation of levels of free intracellular Ca^{2+}. These findings are in line with the decreased Ca^{2+} content of mitochondria also found in these experiments, which indicates impaired mitochondrial Ca^{2+} handling. The changes in intracellular Ca^{2+} handling were accompanied by a hyperpolarized membrane potential, a reduction in action potential frequency, and an increase in the number of POMC neurons with no spontaneous activity. Since the recordings were performed in the presence of synaptic blockers, these alterations in electrophysiological activity were not caused by changes in synaptic input, which have been described previously (*Klöckener et al., 2011*; *Newton et al., 2013*).

Cowley et al. (2001) reported that leptin depolarizes POMC neurons and increases their firing rate; hence, it is conceivable that DIO-induced reduction in intrinsic activity also contributes to leptin resistance. Former studies had primarily focused on defining alterations in leptin-evoked signaling in POMC neurons, revealing ER stress, reduced leptin-evoked Stat-3 phosphorylation, α-MSH secretion in hypothalamic sections of HFD-fed obese mice (*El-Haschimi et al., 2000*), and increased expression of SOCS-3 or fatty acid-induced activation of inhibitory stress kinases (*Belgardt et al., 2010*; *Ernst et al., 2009*; *Kievit et al., 2006*; *Kleinridders et al., 2009*; *Hosoi et al., 2008*; *Ramírez and Claret, 2015*).

Given the results of these previous studies, it is likely that, from a mechanistic point of view, the decreased activity of POMC neurons reflects the net effect of DIO on multiple pathways. Nevertheless, our experiments, in which altering the intracellular Ca^{2+} concentration could reproduce the electrophysiological properties observed in DIO, identified the intracellular Ca^{2+} concentration as a probable direct link between DIO-induced changes in mitochondrial morphology and function, and the reduction in excitability of POMC neurons. Nevertheless, the downstream targets of Ca^{2+} signals have yet to be revealed. Obvious candidates for mediating the observed changes are Ca^{2+} activated K^+ channels (*Kaczorowski et al., 1996*; *Kimm et al., 2015*; *McManus, 1991*; *Pedarzani and Stocker, 2008*; *Sah and Davies, 2000*; *Weatherall et al., 2010*, *Li and Bennett, 2007*; *Liu and Herbison, 2008*). This notion is supported by our experiments which show that the SK channel blocker apamin can, at least in part, revers the Ca^{2+} induced decrease in neuronal activity. Nevertheless, there may well be other Ca^{2+}-dependent pathways that can reduce neuronal excitability (*Ashcroft and Ashcroft, 1990*; *Ha et al., 2016*).

On the systemic level, the clearly decreased activity of POMC neurons represents a critical reduction in, or even loss of, an important satiety signal, which raises questions regarding the etiology of these dramatic changes. One can assume that POMC neurons initially respond to high-fat feeding with an increase in activity in order to prevent a positive energy balance. Subsequently, chronic overactivation could lead to compensatory adaptations to reestablish normal neuronal baseline activity, as it has been demonstrated in numerous neuronal systems (*Marder and Prinz, 2002*). However, the drastic decrease in neuronal activity of anorexic POMC neurons in a situation of sustained high caloric intake clearly argues against a 'controlled' compensatory mechanism aiming at the reestablishment of normal neuronal responses. Considerable Ca^{2+} entry into POMC neurons during sustained activation by HFD might contribute to the impairment of Ca^{2+} homeostasis (*Suyama et al., 2017*). Thus, it seems more likely that the sustained metabolic stress of HFD-feeding directly impairs Ca^{2+}

homeostasis (*Fu et al., 2011*). This notion is in line with previously described alterations in mitochondrial morphology and decreases in mitochondria-ER contacts, caused by downregulation of MNF2 (*Bach et al., 2003*; *Guillet et al., 2011*; *Pich et al., 2005*; *Schneeberger et al., 2013*). This is also interesting in the context of previous work which indicates that an opposite caloric regimen, namely caloric restriction, is an effective way to drastically delay the onset of age related neurodegenerative diseases and age-related impairment of intrinsic neuronal properties (*Hemond and Jaffe, 2005*; *Murchison and Griffith, 2007*). Since several lines of evidence suggest that age-dependent changes in Ca^{2+} homeostasis may increase the susceptibility for age-dependent impairment of neuronal function (*Berridge, 2012*; *Marambaud et al., 2009*; *Toescu and Verkhratsky, 2007*), a compromised Ca^{2+} homeostasis induced by high caloric intake might accelerate aging. Since age-related changes in neuronal activity have also been observed in POMC neurons (*Yang et al., 2012*), the decreased activity observed in our study may be associated with DIO-induced accelerated aging.

From a mechanistic point of view, additional mechanisms have to be taken into account. Since the byproducts of nutrient oxidation are free radicals, and since satiety is associated with high levels of ROS production in POMC neurons, oxidative stress is a likely candidate for modulating mitochondrial function (*Barsukova et al., 2011*). While ROS can act as a physiological signaling molecule at low concentrations (*Brookes et al., 2004*; *Zima and Blatter, 2006*), and while acute increases in ROS levels have been shown to activate POMC neurons (*Diano et al., 2011*), it is not unreasonable to anticipate that sustained high ROS levels as a consequence of high-fat feeding impair mitochondrial function (*Horvath et al., 2009*). At high concentrations, ROS can induce mitochondrial permeability transition, causing mitochondrial Ca^{2+} release and elevation of cytosolic Ca^{2+} levels (*Barsukova et al., 2011*).

In summary, our study shows that DIO dramatically reduces the activity of satiety-mediating POMC neurons. Our experiments suggest that impaired mitochondrial Ca^{2+} handling causes an increase in free cytosolic Ca^{2+}, which mediates membrane hyperpolarization. Our study thus provides direct evidence that besides altering hormonal responses, chronic HFD-feeding induces a direct, profound impairment of cell-intrinsic properties, which are of critical importance for neuronal excitability in energy balance-regulating circuits. Further defining the exact molecular pathways leading to impaired Ca^{2+} handling during the development of diet-induced obesity may thus set the ground for novel therapeutic approaches to tackle the current obesity epidemic.

Materials and methods

Animals and brain slice preparation

All animal procedures were conducted in compliance with guidelines approved by local government authorities (LANUV NRW, Recklinghausen, Germany) and were in accordance with NIH guidelines. Experiments were performed on brain slices from 18-week-old male POMC-EGFP mice that expressed green fluorescent protein (eGFP) selectively in pro-opiomelanocortin (POMC) neurons (*Cowley et al., 2001*). Animals were kept under standard laboratory conditions, with tap water and chow available ad libitum, on a 12 hr light/dark cycle. Animals were either fed normal chow diet (NCD; Teklad Global Rodent 2018; Harlan, Madison, WI, USA) containing 53.5% carbohydrates, 18.5% protein, and 5.5% fat (12% of calories from fat) or a high-fat diet (HFD; C1057; Altromin, Lage, Germany) containing 32.7% carbohydrates, 20% protein, and 35.5% fat (55.2% of calories from fat) for 12 weeks (starting at an age of 6 weeks). The animals were lightly anesthetized with isoflurane (B506; AbbVie Deutschland GmbH and Co KG, Ludwigshafen, Germany) and subsequently decapitated. Coronal slices (270–300 µm) containing the arcuate nucleus of the hypothalamus (ARH) were cut with a vibration microtome (HM-650 V; Thermo Scientific, Walldorf, Germany) under cold (4°C), carbogenated (95% O_2 and 5% CO_2), glycerol-based modified artificial cerebrospinal fluid (GaCSF) (*Ye et al., 2006*). The GaCSF contained (in mM): 250 Glycerol, 2.5 KCl, 2 $MgCl_2$, 2 $CaCl_2$, 1.2 NaH_2PO_4, 10 HEPES, 21 $NaHCO_3$, and 5 Glucose adjusted to pH 7.2 with NaOH. If not mentioned otherwise, the brain slices were continuously superfused with carbogenated aCSF at a flow rate of ~2 ml·min^{-1}. The aCSF contained (in mM): 125 NaCl, 2.5 KCl, 2 $MgCl_2$, 2 $CaCl_2$, 1.2 NaH_2PO_4, 21 $NaHCO_3$, 10 HEPES, and 5 Glucose adjusted to pH 7.2 with NaOH. To block synaptic currents, it contained 10^{-4} M PTX, 5×10^{-5} M D-AP$_5$, and 10^{-5} M CNQX.

Electrophysiology

POMC neurons were recorded at room temperature under current- and voltage-clamp in the perforated patch and whole-cell patch-clamp configuration using an EPC10 patch-clamp amplifier (HEKA, Lambrecht, Germany). Current clamp recordings in the perforated patch configuration were performed using protocols modified from *Horn and Marty (1988)*, *Rae et al. (1991)*, and *Akaike and Harata (1994)*. The recordings were performed with ATP and GTP free pipette solution containing (in mM): 128 K-gluconate, 10 KCl, 10 HEPES, 0.1 EGTA, 2 MgCl$_2$, and adjusted to pH 7.3 with KOH. The patch pipette was tip-filled with internal solution and back-filled with tetraethylrhodamine-dextran (D3308; Invitrogen, Eugene, OR, USA) and amphotericin B (~200 µg·ml^{-1}; A4888; Sigma-Aldrich, Taufkirchen, Germany) or nystatin-containing (~200 µg·ml^{-1}; N6261; Sigma-Aldrich) internal solution to achieve perforated patch recordings. Whole-cell recordings were performed following the methods of Hamill *et al*. (*Hamill et al., 1981*).

Spike frequency adaptation

For SFA ratios 10 s depolarizing stimuli were applied from a holding potential of ~−70 mV with initial instantaneous AP frequencies between 30 and 40 Hz. Instantaneous frequencies were plotted (Y in the next equation) over the 10 s time course and fit to a mono-exponential decay equation with Y_0 set to the initial instantaneous frequency:

$$Y = (Y_0 - \text{Plateau}) \cdot \exp(-K \cdot T) + \text{Plateau}$$

where Plateau is the asymptotic frequency, K the inverse timeconstant and T the time.

Ca^{2+} imaging experiments

For Ca^{2+} imaging experiments, slices were superfused with carbogenated aCSF. To block synaptic currents, it contained 10^{-4} M PTX, 5×10^{-5} M D-AP5, and 10^{-5} M CNQX. The pipette solution contained (in mM): 135 K-gluconate, 10 KCl, 10 HEPES, 2 MgCl$_2$, and 0.1 fura-2 (pentapotassium salt, F1200, Molecular Probes, OR, USA) adjusted with KOH to pH 7.3.

Fluorimetric Ca^{2+} measurements

Intracellular Ca^{2+} concentrations and dynamics were measured with the Ca^{2+} indicator fura-2, a ratiometric dye suitable to determine absolute Ca^{2+} concentration after calibration (*Grynkiewicz et al., 1985*). The Ca^{2+}-handling parameters were determined as described previously using the 'added buffer' approach (*Neher and Augustine, 1992*) in combination with whole-cell patch-clamp recordings and fast optical imaging. The imaging setup consisted of an Imago/SensiCam CCD camera with a 640 × 480 chip (Till Photonics, Gräfelfing, Germany) and a Polychromator IV (Till Photonics) that was coupled via an optical fiber into the upright microscope. The fura-2-loaded neurons were illuminated during data collection with 340 nm, 360 nm, or 380 nm. Emitted fluorescence was detected through a 440 nm long-pass filter (LP440). Data were acquired as 80 × 60 frames using 8 × 8 on-chip binning. Images were recorded in analog-to-digital units (ADUs) and stored and analyzed as 12-bit grayscale images. For all calculations of kinetics, the mean values of ADUs within regions of interest (ROIs) from the center of the cell bodies were used.

Free intracellular Ca^{2+} concentrations were determined as in (*Grynkiewicz et al., 1985*):

$$\left[\text{Ca}^{2+}\right]_i = K_{\text{d,Fura}} \frac{F_{380,\text{min}}}{F_{380,\text{max}}} \cdot \frac{(R - R_{\text{min}})}{(R_{\text{max}} - R)} \tag{1}$$

$\left[\text{Ca}^{2+}\right]_i$ is the free intracellular Ca^{2+} concentration for the background-subtracted fluorescence ratio R from 340 nm and 380 nm excitation. R_{min} and R_{max} are the ratios at a Ca^{2+} concentration of virtually 0 M and at saturating Ca^{2+} concentrations, respectively. $K_{\text{d,Fura}}$ is the dissociation constant of fura-2. $F_{380,\text{min}}/F_{380,\text{max}}$ is the ratio between the emitted fluorescence of Ca^{2+}-free dye and the emitted fluorescence of Ca^{2+}-saturated dye at 380 nm excitation, reflecting the dynamic range of the indicator. The term $K_{\text{d,Fura}} \cdot (F_{380,\text{min}}/F_{380,\text{max}})$ is substituted with the effective dissociation constant $K_{\text{d,Fura},eff}$, which is independent of the dye concentration and specific for each experimental setup:

$$K_{d,\text{Fura,eff}} = \left[\text{Ca}^{2+}\right]_i \frac{(R_{\max} - R)}{(R - R_{\min})} \qquad (2)$$

The free Ca^{2+} concentrations in the calibration solutions were determined using a Ca^{2+}-selective electrode (*Kay et al., 2008*; *McGuigan et al., 1991*). Calibration solutions contained (in mM): $R_{\max}$: 140 KCl, 2.5 KOH, 15 NaCl, 1 MgCl$_2$, 5 HEPES, 10 CaCl$_2$, and 0.05 fura-2; $R_{\min}$: 129.5 KCl, 13 KOH, 15 NaCl, 1 MgCl$_2$, 5 HEPES, 4 EGTA, and 0.05 fura-2; R_{def}: 129.5 KCl, 13 KOH, 10.3 NaCl, 4.7 NaOH, 1 MgCl$_2$, 5 HEPES, 4 EGTA, 2.7 CaCl$_2$, and 0.05 fura-2, yielding a free Ca^{2+} concentration of 0.35 µM. All solutions were adjusted to pH 7.2 with HCl.

Ca^{2+}-handling parameters were determined by using the 'added buffer' approach originally introduced by Neher and Augustine (*Neher and Augustine, 1992*). This method is based on a linear, single compartment model, with the rationale that for measurements of intracellular Ca^{2+} concentrations with Ca^{2+} chelator-based indicators, the amplitude and time course of the signals are dependent on the concentration of the Ca^{2+} indicator (here: fura−2), which acts as an exogenous Ca^{2+} buffer (B), and the endogenous buffer (S). The ability of the experimentally introduced exogenous buffer to bind Ca^{2+} is described by its Ca^{2+}-binding ratio that is defined as the ratio of the change in buffer-bound Ca^{2+} over the change in free Ca^{2+}:

$$\kappa_B = \frac{d[\text{BCa}]}{d\left[\text{Ca}^{2+}\right]_i} = \frac{[\text{B}_T]K_{d,B}}{\left(\left[\text{Ca}^{2+}\right]_i + K_{d,B}\right)^2} \qquad (3)$$

$[\text{B}_T]$ is the total concentration of the exogenous buffer B, and $K_{d,B}$ is its dissociation constant for Ca^{2+}. In this model, the decay time constant ($\tau_{\text{transient}}$) of a Ca^{2+} transient induced by a brief Ca^{2+} influx is described as:

$$\tau_{\text{transient}} = \frac{1 + \kappa_B + \kappa_S}{\gamma - \frac{(1 + \kappa_S)}{\tau_{\text{loading}}}} \qquad (4)$$

$\tau_{\text{transient}}$ is proportional to κ_B, and a linear fit to the data has its negative x-axis intercept at $1 + \kappa_S$, yielding the endogenous Ca^{2+}-binding ratio of the cell. The slope of this fit is the inverse of the Ca^{2+} extrusion rate γ. The y-axis intercept yields the time constant τ_{endo} for the decay of the Ca^{2+} transient as it would appear in the cell without exogenous buffer. $\tau_{\text{transient}}$ values were plotted as a function of κ_B values and fit with a linear function $Y = \beta_0 + \beta_1 x$, using the 'R function' lm (R Development Core Team [2009]). To estimate the variance of the Ca^{2+}-handling parameters, we used the bootstrap method (*Pippow et al., 2009*) implemented in the boot library in R (fixed-x resampling, 1000 bootstrap samples, boot: Bootstrap R Functions, R package version 1.2–36), which provided bootstrap distributions (n = 1000) for each of the parameters. The distributions were log-transformed to bring them closer to a Gaussian. To determine differences in means between the different cell types, unpaired t-tests were performed.

To monitor calcium release from mitochondria into the cytoplasm, the calcium indicator fura-2 was AM-loaded into POMC neurons by incubating brain slices in carbogenated aCSF containing 10 µM fura-2 (fura-2 AM, F1221, Molecular Probes; 24°C for 50–60 min). During the recordings, slices were superfused with aCSF additionally containing 250 µM sulfinpyrazone (S9509, Sigma-Aldrich), to inhibit fura-2 sequestration (*Di Virgilio et al., 1990*). Ca^{2+} release from mitochondria was induced by bath application of 2 µM carbonyl cyanide p-(trifluoromethoxy) phenylhydrazone (FCCP, Sigma-Aldrich) at a flow rate of 3 ml·min^{-1}. Since the background fluorescence is not clearly determinable in AM-loaded cells, no background was subtracted, and instead of reporting absolute changes in free intracellular Ca^{2+}, changes in calcium concentration were given as changes in the fura-2 ratio (340/380 nm) (*Bergmann and Keller, 2004*; *Jaiswal et al., 2009*). For better visualization and comparison of the time courses of the fura-2 ratio between the two populations, we normalized the fluorescence ratio to the baseline. Analysis was performed off-line using IGOR Pro 6 (Wavemetrics, Lake Oswego, OR, USA).

Tools for data analysis and statistics

Electrophysiological data were analyzed using Pulse (version 8.63, HEKA-Elektronik) and Igor Pro six software (Wavemetrics, including the Patcher's Power Tools plug-in: http://www.mpibpc.mpg.de/

groups/neher/index.php?page=software). All calculations for the determination of EGTA purity, its dissociation constant, and the free Ca^{2+} concentrations in the calibration solutions were performed in R (R Development Core Team [2009], http://www.R-project.org). All functions that were used to fit the Ca^{2+} buffering-related data with a linearized one-compartment model were implemented in R (R Development Core Team [2009]. If not stated otherwise, all calculated values are expressed as means ± SEM (standard error of the mean). For pairwise comparisons of dependent and independent normal distributions, paired and unpaired t-tests were used, respectively. For pairwise comparisons of independent, not normal distributions, Mann-Whitney U-tests were used. For multiple comparisons, ANOVA with Bonferroni post hoc analysis was performed. Tests were executed using GraphPad Prism 5 (GraphPad Software Inc., La Jolla, CA, USA). A significance level of 0.05 was accepted for all tests. Significance levels were: $*p<0.05$, $**p<0.01$, $***p<0.001$. In all figures, n-values are given in brackets. Exact p-values are reported if $p>0.0001$.

Acknowledgements

Additional information

Author contributions

LP, Conceptualization, Data curation, Formal analysis, Investigation, Writing—original draft, Writing—review and editing; AP, Conceptualization, Data curation, Formal analysis, Investigation, Writing—review and editing; SH, Formal analysis, Investigation, Writing—review and editing; MP, Formal analysis, Investigation; ACK, AH, Investigation; CP, Software, Formal analysis, Investigation; JCB, Resources, Validation; PK, Conceptualization, Resources, Formal analysis, Supervision, Funding acquisition, Writing—original draft, Project administration, Writing—review and editing

Author ORCIDs

Lars Paeger, http://orcid.org/0000-0001-8716-3483
Christophe Pouzat, http://orcid.org/0000-0002-2844-8099
Peter Kloppenburg, http://orcid.org/0000-0002-4554-404X

Ethics

Animal experimentation: All animal procedures were conducted in compliance with guidelines approved by local government authorities (8.87-51.05.20.09.208, 84-02.05.20.12.254, 8.87-50.10.31.08.279, 84-02.04.2014.A511) (LANUV NRW, Recklinghausen, Germany) and were in accordance with NIH guidelines.

References

Akaike N, Harata N. 1994. Nystatin perforated patch recording and its applications to analyses of intracellular mechanisms. *The Japanese Journal of Physiology* **44**:433–473. doi: 10.2170/jjphysiol.44.433, PMID: 7534361

Apovian CM. 2016. The Obesity Epidemic–understanding the disease and the treatment. *New England Journal of Medicine* **374**:177–179. doi: 10.1056/NEJMe1514957, PMID: 26760089

Ashcroft SJ, Ashcroft FM. 1990. Properties and functions of ATP-sensitive K-channels. *Cellular Signalling* **2**:197–214. doi: 10.1016/0898-6568(90)90048-F, PMID: 2119205

Bach D, Pich S, Soriano FX, Vega N, Baumgartner B, Oriola J, Daugaard JR, Lloberas J, Camps M, Zierath JR, Rabasa-Lhoret R, Wallberg-Henriksson H, Laville M, Palacín M, Vidal H, Rivera F, Brand M, Zorzano A. 2003. Mitofusin-2 determines mitochondrial network architecture and mitochondrial metabolism. A novel regulatory mechanism altered in obesity. *The Journal of Biological Chemistry* **278**:17190–17197. doi: 10.1074/jbc.M212754200, PMID: 12598526

Barsukova A, Komarov A, Hajnóczky G, Bernardi P, Bourdette D, Forte M. 2011. Activation of the mitochondrial permeability transition pore modulates Ca2+ responses to physiological stimuli in adult neurons. *European Journal of Neuroscience* **33**:831–842. doi: 10.1111/j.1460-9568.2010.07576.x, PMID: 21255127

Belgardt BF, Mauer J, Wunderlich FT, Ernst MB, Pal M, Spohn G, Brönneke HS, Brodesser S, Hampel B, Schauss AC, Brüning JC. 2010. Hypothalamic and pituitary c-Jun N-terminal kinase 1 signaling coordinately regulates glucose metabolism. *PNAS* **107**:6028–6033. doi: 10.1073/pnas.1001796107, PMID: 20231445

Belgardt BF, Okamura T, Brüning JC. 2009. Hormone and glucose signalling in POMC and AgRP neurons. *The Journal of Physiology* **587**:5305–5314. doi: 10.1113/jphysiol.2009.179192, PMID: 19770186

Bennett BD, Callaway JC, Wilson CJ. 2000. Intrinsic membrane properties underlying spontaneous tonic firing in neostriatal cholinergic interneurons. *Journal of Neuroscience* **20**:8493–8503. PMID: 11069957

Bergmann F, Keller BU. 2004. Impact of mitochondrial inhibition on excitability and cytosolic Ca2+ levels in brainstem motoneurones from mouse. *The Journal of Physiology* **555**:45–59. doi: 10.1113/jphysiol.2003.053900, PMID: 14660707

Berridge MJ. 2012. Calcium signalling remodelling and disease. *Biochemical Society Transactions* **40**:297–309. doi: 10.1042/BST20110766, PMID: 22435804

Bjørbaek C, Elmquist JK, Frantz JD, Shoelson SE, Flier JS. 1998. Identification of SOCS-3 as a potential mediator of central leptin resistance. *Molecular Cell* **1**:619–625. doi: 10.1016/S1097-2765(00)80062-3, PMID: 9660946

Blatz AL, Magleby KL. 1986. Single apamin-blocked Ca-activated K+ channels of small conductance in cultured rat skeletal muscle. *Nature* **323**:718–720. doi: 10.1038/323718a0, PMID: 2430185

Blouet C, Schwartz GJ. 2010. Hypothalamic nutrient sensing in the control of energy homeostasis. *Behavioural Brain Research* **209**:1–12. doi: 10.1016/j.bbr.2009.12.024, PMID: 20035790

Brenner R, Chen QH, Vilaythong A, Toney GM, Noebels JL, Aldrich RW. 2005. BK channel beta4 subunit reduces dentate gyrus excitability and protects against temporal lobe seizures. *Nature Neuroscience* **8**:1752–1759. doi: 10.1038/nn1573, PMID: 16261134

Brookes PS, Yoon Y, Robotham JL, Anders MW, Sheu SS. 2004. Calcium, ATP, and ROS: a mitochondrial love-hate triangle. *AJP: Cell Physiology* **287**:C817–C833. doi: 10.1152/ajpcell.00139.2004, PMID: 15355853

Claret M, Smith MA, Batterham RL, Selman C, Choudhury AI, Fryer LG, Clements M, Al-Qassab H, Heffron H, Xu AW, Speakman JR, Barsh GS, Viollet B, Vaulont S, Ashford ML, Carling D, Withers DJ. 2007. AMPK is essential for energy homeostasis regulation and glucose sensing by POMC and AgRP neurons. *Journal of Clinical Investigation* **117**:2325–2336. doi: 10.1172/JCI31516, PMID: 17671657

Cowley MA, Smart JL, Rubinstein M, Cerdán MG, Diano S, Horvath TL, Cone RD, Low MJ. 2001. Leptin activates anorexigenic POMC neurons through a neural network in the arcuate nucleus. *Nature* **411**:480–484. doi: 10.1038/35078085, PMID: 11373681

Di Virgilio F, Steinberg TH, Silverstein SC. 1990. Inhibition of Fura-2 sequestration and secretion with organic anion transport blockers. *Cell Calcium* **11**:57–62. doi: 10.1016/0143-4160(90)90059-4, PMID: 2191781

Diano S, Liu ZW, Jeong JK, Dietrich MO, Ruan HB, Kim E, Suyama S, Kelly K, Gyengesi E, Arbiser JL, Belsham DD, Sarruf DA, Schwartz MW, Bennett AM, Shanabrough M, Mobbs CV, Yang X, Gao XB, Horvath TL. 2011. Peroxisome proliferation-associated control of reactive oxygen species sets melanocortin tone and feeding in diet-induced obesity. *Nature Medicine* **17**:1121–1127. doi: 10.1038/nm.2421, PMID: 21873987

Dietrich MO, Liu ZW, Horvath TL. 2013. Mitochondrial dynamics controlled by mitofusins regulate Agrp neuronal activity and diet-induced obesity. *Cell* **155**:188–199. doi: 10.1016/j.cell.2013.09.004, PMID: 24074868

El-Haschimi K, Pierroz DD, Hileman SM, Bjørbaek C, Flier JS. 2000. Two defects contribute to hypothalamic leptin resistance in mice with diet-induced obesity. *Journal of Clinical Investigation* **105**:1827–1832. doi: 10.1172/JCI9842, PMID: 10862798

Ernst MB, Wunderlich CM, Hess S, Paehler M, Mesaros A, Koralov SB, Kleinridders A, Husch A, Münzberg H, Hampel B, Alber J, Kloppenburg P, Brüning JC, Wunderlich FT. 2009. Enhanced Stat3 activation in POMC neurons provokes negative feedback inhibition of leptin and insulin signaling in obesity. *Journal of Neuroscience* **29**:11582–11593. doi: 10.1523/JNEUROSCI.5712-08.2009, PMID: 19759305

Faber ES, Sah P. 2003. Calcium-activated potassium channels: multiple contributions to neuronal function. *The Neuroscientist* **9**:181–194. doi: 10.1177/1073858403009003011, PMID: 15065814

Fioretti B, Castigli E, Calzuola I, Harper AA, Franciolini F, Catacuzzeno L. 2004. NPPB block of the intermediate-conductance Ca2+-activated K+ channel. *European Journal of Pharmacology* **497**:1–6. doi: 10.1016/j.ejphar.2004.06.034, PMID: 15321728

Fu S, Yang L, Li P, Hofmann O, Dicker L, Hide W, Lin X, Watkins SM, Ivanov AR, Hotamisligil GS. 2011. Aberrant lipid metabolism disrupts calcium homeostasis causing liver endoplasmic reticulum stress in obesity. *Nature* **473**:528–531. doi: 10.1038/nature09968, PMID: 21532591

Galvez A, Gimenez-Gallego G, Reuben JP, Roy-Contancin L, Feigenbaum P, Kaczorowski GJ, Garcia ML. 1990. Purification and characterization of a unique, potent, peptidyl probe for the high conductance calcium-activated potassium channel from venom of the scorpion Buthus tamulus. *The Journal of Biological Chemistry* **265**:11083–11173. PMID: 1694175

Gao Q, Horvath TL. 2007. Neurobiology of feeding and energy expenditure. *Annual Review of Neuroscience* **30**: 367–398. doi: 10.1146/annurev.neuro.30.051606.094324, PMID: 17506645

Ghatta S, Nimmagadda D, Xu X, O'Rourke ST. 2006. Large-conductance, calcium-activated potassium channels: structural and functional implications. *Pharmacology & Therapeutics* **110**:103–116. doi: 10.1016/j.pharmthera. 2005.10.007, PMID: 16356551

Giangiacomo KM, Garcia ML, McManus OB. 1992. Mechanism of iberiotoxin block of the large-conductance calcium-activated potassium channel from bovine aortic smooth muscle. *Biochemistry* **31**:6719–6727. doi: 10. 1021/bi00144a011, PMID: 1379069

Grynkiewicz G, Poenie M, Tsien RY. 1985. A new generation of Ca2+ indicators with greatly improved fluorescence properties. *The Journal of Biological Chemistry* **260**:3440–3450. PMID: 3838314

Guillet V, Gueguen N, Cartoni R, Chevrollier A, Desquiret V, Angebault C, Amati-Bonneau P, Procaccio V, Bonneau D, Martinou JC, Reynier P. 2011. Bioenergetic defect associated with mKATP channel opening in a mouse model carrying a mitofusin 2 mutation. *The FASEB Journal* **25**:1618–1627. doi: 10.1096/fj.10-173609, PMID: 21285398

Ha GE, Lee J, Kwak H, Song K, Kwon J, Jung SY, Hong J, Chang GE, Hwang EM, Shin HS, Lee CJ, Cheong E. 2016. The $^{Ca(2+)}$-activated chloride channel anoctamin-2 mediates spike-frequency adaptation and regulates sensory transmission in thalamocortical neurons. *Nature Communications* **7**:13791. doi: 10.1038/ncomms13791, PMID: 27991499

Hamill OP, Marty A, Neher E, Sakmann B, Sigworth FJ. 1981. Improved patch-clamp techniques for high-resolution current recording from cells and cell-free membrane patches. *Pflügers Archiv - European Journal of Physiology* **391**:85–100. doi: 10.1007/BF00656997, PMID: 6270629

Hemond P, Jaffe DB. 2005. Caloric restriction prevents aging-associated changes in spike-mediated Ca2+ accumulation and the slow afterhyperpolarization in hippocampal CA1 pyramidal neurons. *Neuroscience* **135**: 413–420. doi: 10.1016/j.neuroscience.2005.05.044, PMID: 16112472

Horn R, Marty A. 1988. Muscarinic activation of ionic currents measured by a new whole-cell recording method. *The Journal of General Physiology* **92**:145–159. doi: 10.1085/jgp.92.2.145, PMID: 2459299

Horvath TL, Andrews ZB, Diano S. 2009. Fuel utilization by hypothalamic neurons: roles for ROS. *Trends in Endocrinology & Metabolism* **20**:78–87. doi: 10.1016/j.tem.2008.10.003, PMID: 19084428

Hosoi T, Sasaki M, Miyahara T, Hashimoto C, Matsuo S, Yoshii M, Ozawa K. 2008. Endoplasmic reticulum stress induces leptin resistance. *Molecular Pharmacology* **74**:1610–1619. doi: 10.1124/mol.108.050070, PMID: 18755 873

Jaiswal MK, Zech WD, Goos M, Leutbecher C, Ferri A, Zippelius A, Carrì MT, Nau R, Keller BU. 2009. Impairment of mitochondrial calcium handling in a mtSOD1 cell culture model of motoneuron disease. *BMC Neuroscience* **10**:64. doi: 10.1186/1471-2202-10-64, PMID: 19545440

Jo YH, Su Y, Gutierrez-Juarez R, Chua S. 2009. Oleic acid directly regulates POMC neuron excitability in the hypothalamus. *Journal of Neurophysiology* **101**:2305–2316. doi: 10.1152/jn.91294.2008, PMID: 19261705

Jordan SD, Könner AC, Brüning JC. 2010. Sensing the fuels: glucose and lipid signaling in the CNS controlling energy homeostasis. *Cellular and Molecular Life Sciences* **67**:3255–3273. doi: 10.1007/s00018-010-0414-7, PMID: 20549539

Kaczorowski GJ, Knaus HG, Leonard RJ, McManus OB, Garcia ML. 1996. High-conductance calcium-activated potassium channels; structure, pharmacology, and function. *Journal of Bioenergetics and Biomembranes* **28**: 255–267. doi: 10.1007/BF02110699, PMID: 8807400

Kay JW, Steven RJ, McGuigan JA, Elder HY. 2008. Automatic determination of ligand purity and apparent dissociation constant (K(app)) in ca(2+)/Mg(2+) buffer solutions and the K(app) for ca(2+)/Mg(2+) anion binding in physiological solutions from ca(2+)/Mg(2+)-macroelectrode measurements. *Computers in Biology and Medicine* **38**:101–110. doi: 10.1016/j.compbiomed.2007.07.008, PMID: 17854794

Kievit P, Howard JK, Badman MK, Balthasar N, Coppari R, Mori H, Lee CE, Elmquist JK, Yoshimura A, Flier JS. 2006. Enhanced leptin sensitivity and improved glucose homeostasis in mice lacking suppressor of cytokine signaling-3 in POMC-expressing cells. *Cell Metabolism* **4**:123–132. doi: 10.1016/j.cmet.2006.06.010, PMID: 16 890540

Kimm T, Khaliq ZM, Bean BP. 2015. Differential regulation of Action potential shape and Burst-Frequency firing by BK and Kv2 channels in Substantia Nigra Dopaminergic Neurons. *Journal of Neuroscience* **35**:16404–16417. doi: 10.1523/JNEUROSCI.5291-14.2015, PMID: 26674866

Kleinridders A, Schenten D, Könner AC, Belgardt BF, Mauer J, Okamura T, Wunderlich FT, Medzhitov R, Brüning JC. 2009. MyD88 signaling in the CNS is required for development of fatty acid-induced leptin resistance and diet-induced obesity. *Cell Metabolism* **10**:249–259. doi: 10.1016/j.cmet.2009.08.013, PMID: 19808018

Klöckener T, Hess S, Belgardt BF, Paeger L, Verhagen LA, Husch A, Sohn JW, Hampel B, Dhillon H, Zigman JM, Lowell BB, Williams KW, Elmquist JK, Horvath TL, Kloppenburg P, Brüning JC. 2011. High-fat feeding promotes obesity via insulin receptor/PI3K-dependent inhibition of SF-1 VMH neurons. *Nature Neuroscience* **14**:911–918. doi: 10.1038/nn.2847, PMID: 21642975

Könner AC, Brüning JC. 2012. Selective insulin and leptin resistance in metabolic disorders. *Cell Metabolism* **16**: 144–152. doi: 10.1016/j.cmet.2012.07.004, PMID: 22883229

Könner AC, Janoschek R, Plum L, Jordan SD, Rother E, Ma X, Xu C, Enriori P, Hampel B, Barsh GS, Kahn CR, Cowley MA, Ashcroft FM, Brüning JC. 2007. Insulin action in AgRP-expressing neurons is required for suppression of hepatic glucose production. *Cell Metabolism* **5**:438–449. doi: 10.1016/j.cmet.2007.05.004, PMID: 17550779

Li G, Cheung DW. 1999. Effects of paxilline on K+ channels in rat mesenteric arterial cells. *European Journal of Pharmacology* **372**:103–107. doi: 10.1016/S0014-2999(99)00188-0, PMID: 10374720

Li X, Bennett DJ. 2007. Apamin-sensitive calcium-activated potassium currents (SK) are activated by persistent calcium currents in rat motoneurons. *Journal of Neurophysiology* **97**:3314–3330. doi: 10.1152/jn.01068.2006, PMID: 17360829

Liu X, Herbison AE. 2008. Small-conductance calcium-activated potassium channels control excitability and firing dynamics in gonadotropin-releasing hormone (GnRH) neurons. *Endocrinology* **149**:3598–3604. doi: 10.1210/en.2007-1631, PMID: 18372332

Marambaud P, Dreses-Werringloer U, Vingtdeux V. 2009. Calcium signaling in neurodegeneration. *Molecular Neurodegeneration* **4**:20. doi: 10.1186/1750-1326-4-20, PMID: 19419557

Marder E, Prinz AA. 2002. Modeling stability in neuron and network function: the role of activity in homeostasis. *BioEssays* **24**:1145–1154. doi: 10.1002/bies.10185, PMID: 12447979

McGuigan JA, Lüthi D, Buri A. 1991. Calcium buffer solutions and how to make them: a do it yourself guide. *Canadian Journal of Physiology and Pharmacology* **69**:1733–1749. doi: 10.1139/y91-257, PMID: 1804518

McManus OB. 1991. Calcium-activated potassium channels: regulation by calcium. *Journal of Bioenergetics and Biomembranes* **23**:537–560. doi: 10.1007/BF00785810, PMID: 1917908

Morton GJ, Cummings DE, Baskin DG, Barsh GS, Schwartz MW. 2006. Central nervous system control of food intake and body weight. *Nature* **443**:289–295. doi: 10.1038/nature05026, PMID: 16988703

Murchison D, Griffith WH. 2007. Calcium buffering systems and calcium signaling in aged rat basal forebrain neurons. *Aging Cell* **6**:297–305. doi: 10.1111/j.1474-9726.2007.00293.x, PMID: 17517040

Neher E, Augustine GJ. 1992. Calcium gradients and buffers in bovine chromaffin cells. *The Journal of Physiology* **450**:273–301. doi: 10.1113/jphysiol.1992.sp019127, PMID: 1331424

Newton AJ, Hess S, Paeger L, Vogt MC, Fleming Lascano J, Nillni EA, Brüning JC, Kloppenburg P, Xu AW. 2013. AgRP innervation onto POMC neurons increases with age and is accelerated with chronic high-fat feeding in male mice. *Endocrinology* **154**:172–183. doi: 10.1210/en.2012-1643, PMID: 23161869

Parton LE, Ye CP, Coppari R, Enriori PJ, Choi B, Zhang CY, Xu C, Vianna CR, Balthasar N, Lee CE, Elmquist JK, Cowley MA, Lowell BB. 2007. Glucose sensing by POMC neurons regulates glucose homeostasis and is impaired in obesity. *Nature* **449**:228–232. doi: 10.1038/nature06098, PMID: 17728716

Pedarzani P, Stocker M. 2008. Molecular and cellular basis of small–and intermediate-conductance, calcium-activated potassium channel function in the brain. *Cellular and Molecular Life Sciences* **65**:3196–3217. doi: 10.1007/s00018-008-8216-x, PMID: 18597044

Penn Y, Segal M, Moses E. 2016. Network synchronization in hippocampal neurons. *PNAS* **113**:3341–3346. doi: 10.1073/pnas.1515105113, PMID: 26961000

Pich S, Bach D, Briones P, Liesa M, Camps M, Testar X, Palacín M, Zorzano A. 2005. The Charcot-marie-tooth type 2A gene product, Mfn2, up-regulates fuel oxidation through expression of OXPHOS system. *Human Molecular Genetics* **14**:1405–1415. doi: 10.1093/hmg/ddi149, PMID: 15829499

Pineda JC, Galarraga E, Bargas J, Cristancho M, Aceves J. 1992. Charybdotoxin and apamin sensitivity of the calcium-dependent repolarization and the afterhyperpolarization in neostriatal neurons. *Journal of Neurophysiology* **68**:287–294. PMID: 1381420

Pippow A, Husch A, Pouzat C, Kloppenburg P. 2009. Differences of Ca2+ handling properties in identified central olfactory neurons of the antennal lobe. *Cell Calcium* **46**:87–98. doi: 10.1016/j.ceca.2009.05.004, PMID: 19545897

Power ML. 2012. The human obesity epidemic, the mismatch paradigm, and our modern "captive" environment. *American Journal of Human Biology* **24**:116–122. doi: 10.1002/ajhb.22236, PMID: 22287210

Rae J, Cooper K, Gates P, Watsky M. 1991. Low access resistance perforated patch recordings using amphotericin B. *Journal of Neuroscience Methods* **37**:15–26. doi: 10.1016/0165-0270(91)90017-T, PMID: 2072734

Ramírez S, Claret M. 2015. Hypothalamic ER stress: a bridge between leptin resistance and obesity. *FEBS Letters* **589**:1678–1687. doi: 10.1016/j.febslet.2015.04.025, PMID: 25913783

Rizzuto R, De Stefani D, Raffaello A, Mammucari C. 2012. Mitochondria as sensors and regulators of calcium signalling. *Nature Reviews Molecular Cell Biology* **13**:566–578. doi: 10.1038/nrm3412, PMID: 22850819

Rowland AA, Voeltz GK. 2012. Endoplasmic reticulum-mitochondria contacts: function of the junction. *Nature Reviews Molecular Cell Biology* **13**:607–625. doi: 10.1038/nrm3440, PMID: 22992592

Sah P, Davies P. 2000. Calcium-activated potassium currents in mammalian neurons. *Clinical and Experimental Pharmacology and Physiology* **27**:657–663. doi: 10.1046/j.1440-1681.2000.03317.x, PMID: 10972528

Sanchez M, McManus OB. 1996. Paxilline inhibition of the alpha-subunit of the high-conductance calcium-activated potassium channel. *Neuropharmacology* **35**:963–968. doi: 10.1016/0028-3908(96)00137-2, PMID: 8938726

Santo-Domingo J, Demaurex N. 2010. Calcium uptake mechanisms of mitochondria. *Biochimica Et Biophysica Acta (BBA) - Bioenergetics* **1797**:907–912. doi: 10.1016/j.bbabio.2010.01.005, PMID: 20079335

Schneeberger M, Dietrich MO, Sebastián D, Imbernón M, Castaño C, Garcia A, Esteban Y, Gonzalez-Franquesa A, Rodríguez IC, Bortolozzi A, Garcia-Roves PM, Gomis R, Nogueiras R, Horvath TL, Zorzano A, Claret M. 2013. Mitofusin 2 in POMC neurons connects ER stress with leptin resistance and energy imbalance. *Cell* **155**:172–187. doi: 10.1016/j.cell.2013.09.003, PMID: 24074867

Schwartz MW, Porte D. 2005. Diabetes, obesity, and the brain. *Science* **307**:375–379. doi: 10.1126/science.1104344, PMID: 15662002

Sohn JW, Elmquist JK, Williams KW. 2013. Neuronal circuits that regulate feeding behavior and metabolism. *Trends in Neurosciences* **36**:504–512. doi: 10.1016/j.tins.2013.05.003, PMID: 23790727

Spanswick D, Smith MA, Groppi VE, Logan SD, Ashford ML. 1997. Leptin inhibits hypothalamic neurons by activation of ATP-sensitive potassium channels. *Nature* **390**:521–525. doi: 10.1038/37379, PMID: 9394003

Spanswick D, Smith MA, Mirshamsi S, Routh VH, Ashford ML. 2000. Insulin activates ATP-sensitive K+ channels in hypothalamic neurons of lean, but not obese rats. *Nature Neuroscience* **3**:757–758. doi: 10.1038/77660, PMID: 10903566

Steculorum SM, Paeger L, Bremser S, Evers N, Hinze Y, Idzko M, Kloppenburg P, Brüning JC. 2015. Hypothalamic UDP increases in obesity and promotes Feeding via P2Y6-dependent activation of AgRP neurons. *Cell* **162**:1404–1417. doi: 10.1016/j.cell.2015.08.032, PMID: 26359991

Steculorum SM, Ruud J, Karakasilioti I, Backes H, Engström Ruud L, Timper K, Hess ME, Tsaousidou E, Mauer J, Vogt MC, Paeger L, Bremser S, Klein AC, Morgan DA, Frommolt P, Brinkkötter PT, Hammerschmidt P, Benzing T, Rahmouni K, Wunderlich FT, et al. 2016. AgRP neurons Control systemic insulin sensitivity via myostatin expression in brown adipose tissue. *Cell* **165**:125–138. doi: 10.1016/j.cell.2016.02.044, PMID: 27015310

Su H, Alroy G, Kirson ED, Yaari Y. 2001. Extracellular calcium modulates persistent sodium current-dependent burst-firing in hippocampal pyramidal neurons. *Journal of Neuroscience* **21**:4173–4182. PMID: 11404402

Surmeier DJ, Guzman JN, Sanchez-Padilla J. 2010. Calcium, cellular aging, and selective neuronal vulnerability in Parkinson's disease. *Cell Calcium* **47**:175–182. doi: 10.1016/j.ceca.2009.12.003, PMID: 20053445

Suyama S, Ralevski A, Liu ZW, Dietrich MO, Yada T, Simonds SE, Cowley MA, Gao XB, Diano S, Horvath TL. 2017. Plasticity of calcium-permeable AMPA glutamate receptors in Pro-opiomelanocortinneurons. *eLife* **6**: e25755. doi: 10.7554/eLife.25755

Szabadkai G, Duchen MR. 2008. Mitochondria: the hub of cellular Ca2+ signaling. *Physiology* **23**:84–94. doi: 10.1152/physiol.00046.2007, PMID: 18400691

Toescu EC, Verkhratsky A. 2007. The importance of being subtle: small changes in calcium homeostasis control cognitive decline in normal aging. *Aging Cell* **6**:267–273. doi: 10.1111/j.1474-9726.2007.00296.x, PMID: 17517038

Tsaousidou E, Paeger L, Belgardt BF, Pal M, Wunderlich CM, Brönneke H, Collienne U, Hampel B, Wunderlich FT, Schmidt-Supprian M, Kloppenburg P, Brüning JC. 2014. Distinct roles for JNK and IKK activation in Agouti-Related peptide neurons in the development of obesity and insulin resistance. *Cell Reports* **9**:1495–1506. doi: 10.1016/j.celrep.2014.10.045, PMID: 25456138

Ueki K, Kondo T, Kahn CR. 2004. Suppressor of cytokine signaling 1 (SOCS-1) and SOCS-3 cause insulin resistance through inhibition of tyrosine phosphorylation of insulin receptor substrate proteins by discrete mechanisms. *Molecular and Cellular Biology* **24**:5434–5446. doi: 10.1128/MCB.24.12.5434-5446.2004, PMID: 15169905

Vandael DH, Zuccotti A, Striessnig J, Carbone E. 2012. Ca(V)1.3-driven SK channel activation regulates pacemaking and spike frequency adaptation in mouse chromaffin cells. *Journal of Neuroscience* **32**:16345–16359. doi: 10.1523/JNEUROSCI.3715-12.2012, PMID: 23152617

Varela L, Horvath TL. 2012. Leptin and insulin pathways in POMC and AgRP neurons that modulate energy balance and glucose homeostasis. *EMBO Reports* **13**:1079–1086. doi: 10.1038/embor.2012.174, PMID: 23146889

Weatherall KL, Goodchild SJ, Jane DE, Marrion NV. 2010. Small conductance calcium-activated potassium channels: from structure to function. *Progress in Neurobiology* **91**:242–255. doi: 10.1016/j.pneurobio.2010.03.002, PMID: 20359520

Wolfart J, Neuhoff H, Franz O, Roeper J. 2001. Differential expression of the small-conductance, calcium-activated potassium channel SK3 is critical for pacemaker control in dopaminergic midbrain neurons. *Journal of Neuroscience* **21**:3443–3456. PMID: 11331374

Yang SB, Tien AC, Boddupalli G, Xu AW, Jan YN, Jan LY. 2012. Rapamycin ameliorates age-dependent obesity associated with increased mTOR signaling in hypothalamic POMC neurons. *Neuron* **75**:425–436. doi: 10.1016/j.neuron.2012.03.043, PMID: 22884327

Ye JH, Zhang J, Xiao C, Kong JQ. 2006. Patch-clamp studies in the CNS illustrate a simple new method for obtaining viable neurons in rat brain slices: glycerol replacement of NaCl protects CNS neurons. *Journal of Neuroscience Methods* **158**:251–259. doi: 10.1016/j.jneumeth.2006.06.006, PMID: 16842860

Yen JC, Chan JY, Chan SH. 1999. Involvement of apamin-sensitive SK channels in spike frequency adaptation of neurons in nucleus tractus solitarii of the rat. *Journal of Biomedical Science* **6**:418–424. doi: 10.1007/BF02253673, PMID: 10545777

Zhou Y, Lingle CJ. 2014. Paxilline inhibits BK channels by an almost exclusively closed-channel block mechanism. *The Journal of General Physiology* **144**:415–440. doi: 10.1085/jgp.201411259, PMID: 25348413

Zima AV, Blatter LA. 2006. Redox regulation of cardiac calcium channels and transporters. *Cardiovascular Research* **71**:310–321. doi: 10.1016/j.cardiores.2006.02.019, PMID: 16581043